A kinetic modeling framework for the peroxide-initiated radical polymerization of styrene in the presence of rubber particles from recycled tires

Dimitrios Meimaroglou, Daniela Florez, Guo-Hua Hu

Version of Record: https://www.sciencedirect.com/science/article/pii/S0009250921007028
Manuscript_00118d6d4f8abddb4b67de2ec9c5da39

A kinetic modeling framework for the peroxide-initiated radical polymerization of styrene in the presence of rubber particles from recycled tires

Dimitrios Meimaroglou*, Daniela Florez[1], Guo-Hua Hu

Laboratoire Réactions et Génie des Procédés,Université de Lorraine,CNRS, LRGP, F-54000 Nancy, France

Abstract

A novel modeling framework is presented for the peroxide-initiated radical polymerization of styrene, in the presence of ground-tire rubber particles. The model takes into account the previously observed effects of the rubber particles, and their highly-reactive additives, on the course of the polymerization. To this end, a generalized kinetic mechanism is proposed, on the basis of a typical styrene homopolymerization scheme, including also a series of additional chemical reactions that are implemented to describe the deviation of the system from the respective homopolymerization case when ground-tire rubber is present in the mixture. This deviation is mainly manifested through an accelerated peroxide decomposition and significant retardation and inhibition of the reaction and displays a non-linear dependence on the contents of rubber particles and initiator. The proposed model succeeds in predicting this behavior under different reaction conditions, while its generality makes it

*Corresponding author
Email address: dimitrios.meimaroglou@univ-lorraine.fr (Dimitrios Meimaroglou)
[1]current address: 7 Le Beaulieu, les Voivres, 88240, France

suitable for implementation in other similar grafting polymerization systems.

Keywords: styrene, radical polymerization, ground-tire rubber, kinetic model, method of moments, peroxide

---

1. Introduction

Automobile tires constitute an irreplaceable product of modern everyday life and an example of continuous scientific research and advancements in terms of its durability and performance. At the same time, they also constitute a significant source of pollution since an important part of end-of-life tires (i.e., tires that can no longer be used on automobiles, even after retreading) end-up in land fills or are burnt for energy recovery. Hence, an increasing scientific interest is nowadays directed towards the exploitation of eventual solutions to this ecological problem [1, 2, 3]. This need is further amplified by the increasing global demand in reducing, reusing and recycling plastic waste, since a significant proportion of tires is composed of a mixture of elastomers (i.e., rubber) [4].

In this respect, a promising solution consists in mechanically grinding the rubber part of tires, after removal of tissue and metallic parts, to form a powder of micrometric particles that can be subsequently used as raw material for new products and applications. For example, this powder, which is commercially called Ground Tire Rubber, GTR, is often used to modify the mechanical properties of new polymeric materials. For instance, it can be employed as a filler of otherwise brittle polymers, such as polystyrene (PS) [5], to improve their stress cracking resistance and their impact strength [1, 6, 7].

The addition of pure rubber particles of nanometric size to the matrix of PS, a brittle thermoplastic commodity polymer of a very wide range of applications, is a well-established commercial process that imparts significant strength to the final polymeric product, commercially known as high-impact polystyrene (HIPS) [4, 5, 8]. Accordingly, an idea that has been followed by several research studies focuses on replacing the fresh rubber with GTR particles in an attempt to achieve a similar improvement in the mechanical properties of polystyrene [9, 10, 11]. This idea is even more interesting as it promotes, at the same time, the recycling of used tires within a general sustainability perspective.

However, a simple mixing of the two materials (i.e., of pure PS and GTR) does not result in the expected outcome as the two phases display low adhesion towards one another. Hence, the produced blend is highly heterogeneous, with respect to the dispersion of the GTR particles within the PS matrix, thus severely limiting the improvement of its stress cracking resistance. Several solutions have been proposed to overcome this low adhesion by targeting its main sources, including compatibilization techniques and surface modification treatments of GTR. Among them, a particularly interesting strategy is to render the two phases compatible by grafting the polymer directly onto the surface of the GTR particles via in-situ radical polymerization [1, 12, 11].

When particulate fillers are present in radical polymerization systems, they may often interact with other reactive species that are present in the mixture, thus affecting the kinetic developments and the overall course of the polymerization. The degree to which these effects may be more or less pronounced depends mainly on the filler's physicochemical characteristics as

well as on the nature of the system. As a result, the polymerization may be mildly or significantly accelerated or retarded, in terms of the evolution of the monomer conversion and/or the chain length characteristics, by the presence of a filler that displays strong interactions with other reactive components of the system (e.g., the monomer(s) or the initiator agent(s)) [4, 13, 14].

GTR has been shown to display such effects when present in radical polymerization systems. For example, when added to acrylate polymerization systems, such as methyl methacrylate (MMA), glycidyl methacrylate (GMA) and hydroxy ethyl methacrylate (HEMA), initiated using benzoyl-peroxide (BPO), an acceleration of the course of the polymerization was observed [13]. At the same time, the presence of GTR in the radical polymerization of styrene displayed an overall inhibition effect, when BPO was used as initiator, but when an azo-initiator, such as azobis(isobutyronitrile) (AIBN), was used instead of BPO, its impact was merely observed [11, 15]. Previous studies [13, 16, 17, 18, 19, 20, 21, 22] have pointed out that important interactions may take place between peroxide initiators and active groups that exist on the surface of carbon black (see Scheme 1), the most widespread reinforcing agent of rubber tires. However, these interactions may be of different nature and extent in different reactive systems. In this respect, the way in which GTR may affect the course of the polymerization, displaying an overall accelerating or inhibiting effect on different polymerization systems, has been attributed [13, 23] to the e-value of the monomers, which is characteristic of their polarity and reactivity, as defined in the original work of Alfrey and Price [24].

In an attempt to elucidate these effects, differential scanning calorimetry

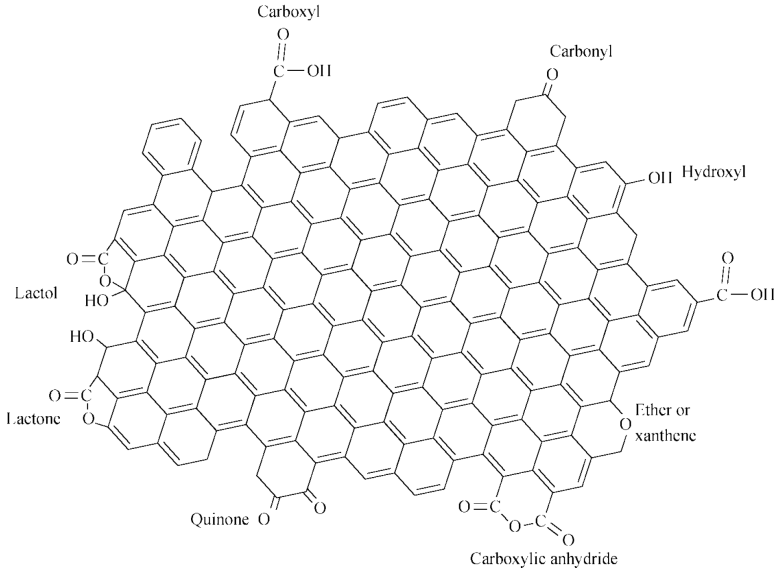

Scheme 1: Aromatic layer plane of carbon black with different functional groups [25].

(DSC) has been used, in the framework of a previous work, to study the bulk radical polymerization of styrene in the presence of different amounts of GTR [23]. The results of that study confirmed that the presence of GTR displays a significant inhibition effect on the course of the peroxide-initiated polymerization. They also revealed that these effects were more pronounced at GTR content of around 30% wt and that a further increase of its content did not necessarily aggravate the observed inhibition effects, thus suggesting the interplay of "coverage" or "masking" phenomena of the carbon black surface active groups, a phenomenon similar to the saturation of the surface of catalysts, observed in catalytic systems. Finally, the findings of that study, including the calculation of the apparent activation energy of the polymerization under the different tested conditions, were also in line with a previously

reported effect of accelerated decomposition of peroxide initiators, also induced by the presence of carbon black [13, 16].

Following up on that experimental study, this work presents a comprehensive modeling framework for the radical bulk polymerization of styrene that is consistent with the observed evolution of the system, both in the absence and in the presence of GTR. The proposed model is based on an extended kinetic scheme that includes the typical chemical reactions that are commonly encountered in styrene homopolymerization studies, as well as chemical reactions that have been introduced to simulate the effects observed when GTR is added to the system. For the calibration and the validation of the model, a series of experimental data have been collected from different literature studies, initially corresponding only to the case of pure styrene homopolymerization. These data were then enriched with additional experimental data produced in the framework of this study, including DSC measurements [23] and bench-scale solution polymerization runs [26], both in the presence and in the absence of GTR.

The mathematical modeling of the radical polymerization of styrene has been extensively studied and several modeling frameworks have been proposed. The reported works of the group of Hamielec [27, 28, 29, 30], as well as the work of Mayo [31], were certainly pioneering in the domain and have set the grounds for later modeling developments. In the following years, the diffusion-controlled phenomena, governing the termination, propagation and initiation reactions, were also extensively analyzed and different models were proposed to describe them [32, 33, 34]. Among the relatively more recent studies, one can distinguish the works published by Penlidis [35, 36], Ko-

toulas et al. [37] and, more recently, Woloszyn [38, 39], since they present accurate models combining thermal and chemical initiation mechanisms and diffusion phenomena, explore the cases of multifunctional initiators and focus on parametric identification problems.

Several studies are also reported for the modeling of styrene radical polymerization including grafting mechanisms. A very early study, published by Manaresi et al. [40], presented a kinetic mechanism that included grafting reactions of styrene on pure 1,4-polybutadiene and a corresponding kinetic model. A series of relevant studies has also been published by Cameron and coworkers, extending over a long period of time and including different systems in terms of rubber polymers (e.g., polybutadiene and polyisoprene) and monomers (e.g., styrene and methyl-methacrylate) [12, 41, 42]. Similarly, Huang and Sundberg [43, 44, 45, 46] published a series of studies on the grafting mechanisms of different monomers (i.e., styrene, methyl acrylate and methyl methacrylate) on polybutadiene, in the presence of various initiators and on the basis of a detailed kinetic mechanism, including homopolymerization and grafting reactions. Meira and coworkers also presented detailed kinetic models on the production process of high-impact polystyrene (HIPS) [47, 8]. Very recently, the groups of d'Hooge, Zhou and Luo published two relevant studies, one using Monte Carlo for the prediction of the molecular topology of the grafting products for single phase grafting of polybutadiene with styrene ([48]) and another one investigating advanced parametric estimation routes for the same system ([49]). Other modeling studies can also be found in the relevant literature, with slight modifications in terms of the reacting components and/or the process [50, 51, 52]. In certain cases, inhibition

reactions were also included in the proposed kinetic mechanisms to account for the effect of impurities, or other additives, that could be present in the mixture and could lead to the termination of growing radicals [8]. However, to the best of the authors' knowledge, the presence of used tire rubber particles in the styrene radical polymerization system has not yet been addressed by any modeling study. Note that, as mentioned above, GTR is a mixture of different rubbers and additives whose exact composition and structure are often unknown. This is a major difference with respect to the aforementioned works on well-identified elastomers. The present work is the first attempt to propose a complete kinetic modeling framework of this system, capable of describing the evolution of the polymerization both in the absence (i.e., homopolymerization case) and in the presence of used tire particles as well as the effects of the contents of the GTR and additives on the course of the polymerization.

2. Experimental

2.1. DSC experiments

All DSC measurements were carried out in a Q2000 calorimeter of TA Instruments, using hermetic aluminum pans, specifically adapted for volatile products. Two consecutive isothermal scans were performed with an intermediate cooling step down to 50 °C. All the reagents used, namely, styrene monomer (with a purity $\geq$ 99.5% and stabilized with $\sim$ 0.005% of 4-tert-butylcatechol) and BPO (75%, remainder water), were purchased from Sigma-Aldrich and used without further purification. Commercial GTR, in the form of powder, was obtained from DeltaGom France and was used without pu-

rification. The relevant details about the sample preparation process, the scanning and recording details, as well as the exploitation of the recorded data, can be found elsewhere [23].

2.2. Bench-scale polymerization experiments

Isothermal solution homopolymerization of styrene, in toluene, was carried out in an agitated batch reactor of total volume capacity of 1 liter [26]. Styrene was purified, prior to the polymerization, by filtration in an aluminum oxide (Al_2O_3) column. The initial mass of toluene in the system was equal to that of styrene in all experiments. Polymerizations were performed at 80 °C and 90 °C. BPO was previously dissolved in the solvent and the mixture was introduced in the reactor and purged with nitrogen atmosphere during 20 minutes under permanent agitation. Subsequently, the monomer was added and the medium was heated to the reaction temperature at 2 °C /min. The total reaction time was 4 to 6 h, under permanent stirring at 300 rpm. The degree of monomer conversion was measured by gravimetry and the number- and weight-average molecular weights were determined by size exclusion chromatography (SEC), using a refractive index Obtilab REX (RI) detector and a multi-angle light scattering MALS WYATT mini dawn TREOS detector, in combination with three separation columns PLgel with pore sizes of 100 Å, 1000 Å and 10^5 Å. Measurements were carried out at a flow rate of 1 mL/min in THF at 40 °C, at a concentration of about 6 to 8 mg/mL.

3. Polymerization kinetic mechanism

The following kinetic scheme was employed to account for all possible reactions taking place in the system, both in the absence and in the presence of GTR:

- Chemical initiation
  - Thermal decomposition of initiator:

$$I \xrightarrow{k_d, f_1} 2PR \tag{1}$$

  - Decomposition of initiator induced by carbon black:

$$I + CB \xrightarrow{k_{dCB}, f_2} PRl \tag{2}$$

  - Free radical initiation:

$$M + PR \xrightarrow{k_I} R_1 \tag{3}$$

  - Formation of grafted primary radicals:

$$G + PR \xrightarrow{k_{IG}} GPR \tag{4}$$

  - Grafted radical initiation:

$$M + GPR \xrightarrow{k_{pG}} GR_1 \tag{5}$$

  - Initiation of reduced-activity free radicals:

$$M + PRl \xrightarrow{\alpha \cdot k_I} P_1 \tag{6}$$

– Initiation of reduced-activity grafted radicals:

$$G + PRl \xrightarrow{\alpha \cdot k_{IG}} GP_1 \tag{7}$$

- Thermal initiation

  – Diels-Alder dimerization of styrene:

$$2M \underset{k_{-1}}{\overset{k_1}{\longleftrightarrow}} AH \tag{8}$$

  – Initiation from Diels-Alder adduct (AH):

$$AH + M \xrightarrow{k_2} AR + MR \tag{9}$$

  – Initiation from 1-phenyltetralyl radical (AR):

$$AR + M \xrightarrow{k_A} R_3 \tag{10}$$

  – Initiation from styryl radical (MR):

$$MR + M \xrightarrow{k_B} R_2 \tag{11}$$

  – Trimerization reaction of Diels-Alder adduct:

$$AH + M \xrightarrow{k_C} D_3 \tag{12}$$

- Propagation:

  – of free radicals:

$$M + R_n \xrightarrow{k_p} R_{n+1} \tag{13}$$

  – of grafted radicals:

$$M + GR_n \xrightarrow{k_{pG}} GR_{n+1} \tag{14}$$

– of reduced-activity free radicals:

$$M + P_n \xrightarrow{\alpha \cdot k_p} P_{n+1} \tag{15}$$

– of reduced-activity grafted radicals:

$$M + GP_n \xrightarrow{\alpha \cdot k_{pG}} GP_{n+1} \tag{16}$$

- Transfer:

  – to monomer from free radicals:

$$M + R_n \xrightarrow{k_{fm}} D_n + R_1 \tag{17}$$

  – to adduct from free radicals:

$$AH + R_n \xrightarrow{k_{fAH}} D_n + AR \tag{18}$$

  – to monomer from grafted radicals:

$$M + GR_n \xrightarrow{k_{fmG}} GD_n + R_1 \tag{19}$$

  – to adduct from grafted radicals:

$$AH + GR_n \xrightarrow{k_{fAHG}} GD_n + AR \tag{20}$$

  – to GTR from free radicals:

$$G + R_n \xrightarrow{k_{fG}} D_n + GPR \tag{21}$$

- Scission (induced by primary-radicals):

  - of free polymer

$$PR + D_n \xrightarrow{k_s} R_m + D_{n-m} \tag{22}$$

  - of grafted polymer

$$PR + GD_n \xrightarrow{k_{sG}} R_m + GD_{n-m} \tag{23}$$

- Termination:

  - by combination of free radicals

$$R_n + R_m \xrightarrow{k_{tc}} D_{n+m} \tag{24}$$

  - by disproportionation of free radicals

$$R_n + R_m \xrightarrow{k_{td}} D_n + D_m \tag{25}$$

  - by combination between free and grafted radicals

$$R_n + GR_m \xrightarrow{k_{tcG}} GD_{n+m} \tag{26}$$

  - by disproportionation between free and grafted radicals

$$R_n + GR_m \xrightarrow{k_{tdG}} D_n + GD_m \tag{27}$$

  - between free and reduced-activity radicals

$$R_n + P_m \xrightarrow{\alpha \cdot k_{tc/td}} D_{n+m}/D_n + D_m \tag{28}$$

  - between grafted and reduced-activity radicals

$$GR_n + P_m \xrightarrow{\alpha \cdot k_{tcG/tdG}} GD_{n+m}/GD_n + D_m \tag{29}$$

- between free and reduced-activity grafted radicals

$$R_n + GP_m \xrightarrow{\alpha \cdot k_{tcG/tdG}} GD_{n+m}/D_n + GD_m \tag{30}$$

- between reduced-activity radicals

$$P_n + P_m \xrightarrow{\alpha^2 \cdot k_{tc/td}} D_{n+m}/D_n + D_m \tag{31}$$

- between free and primary-radicals

$$R_n + PR \xrightarrow{k_{tPR}} D_n \tag{32}$$

- between grafted and primary-radicals

$$GR_n + PR \xrightarrow{k_{tPRG}} GD_n \tag{33}$$

- Radical deactivation by carbon black:

  - of primary-radicals

$$PR/GPR + CB \xrightarrow{k_{dea}} DPR \tag{34}$$

  - of MR radicals

$$MR + CB \xrightarrow{k_{dea}} D_1 \tag{35}$$

  - of AR radicals

$$AR + CB \xrightarrow{k_{dea}} D_2 \tag{36}$$

  - of free radicals

$$CB + R_n \xrightarrow{k_{dea}} D_n \tag{37}$$

  - of grafted radicals

$$CB + GR_n \xrightarrow{k_{deaG}} GD_n \tag{38}$$

– of reduced-activity free radicals

$$CB + P_n \xrightarrow{\alpha \cdot k_{dea}} D_n \tag{39}$$

– of reduced-activity grafted radicals

$$CB + GP_n \xrightarrow{\alpha \cdot k_{deaG}} GD_n \tag{40}$$

All symbols are described in the Nomenclature (section 7). The postulated kinetic scheme contains all the chemical reactions that are commonly encountered in studies of the radical polymerization of styrene, including both chemical and thermal initiation mechanisms (i.e., reactions (1), (3), (8)-(12)), propagation, transfer and termination reactions (i.e., reactions (13), (17)-(18), (32), and (24)-(25)), as well as scission reactions by primary radicals (i.e., reaction (22)), as reported in some studies [38, 39]. Note that, a much simpler thermal initiation mechanism has been proposed by Hui and Hamielec [29], employing a single kinetic chemical reaction. Although this mechanism is attractive and has been adopted by several subsequent studies, it limits the flexibility of the model in terms of its possibility to track the intermediate species, such as the Diels-Alder adduct, which may participate in other reactions (e.g., transfer reactions). Thus, the complete thermal initiation mechanism, reported in Kotoulas et al. [37] and in other similar modeling studies [38, 39], has been adopted in this work.

In addition to the above, a series of additional chemical reactions are included in this general kinetic scheme to simulate the kinetic developments taking place in the system in the presence of GTR, which is taken into account by considering its chemical groups, exposed to the rest of the reacting

species, denoted as G in the above equations. These reactions have been employed in accordance to the effects observed previously and reported in the literature [13, 23]. More specifically, these effects can be broadly classified into two general categories. The first one includes the grafting reactions, describing the formation of radicals on the surface of the GTR particles and their subsequent participation in the polymerization reactions (i.e., reactions (4)-(5), (7), (14), (16), (19)-(21), (33), (23), (26)-(27), (29)-(30), (34), (38) and (40)). The second category includes the reactions of catalyzed decomposition of the initiator (i.e., reaction (2)) and radical deactivation (i.e, reactions (34)-(40)), both induced by the presence of carbon black in the formulation of GTR. The observed retardation effect, also attributed to the presence of carbon black [13, 17, 16], has been included in the kinetic scheme by the fact that the carbon black-induced initiation leads to the formation of radicals of reduced activity with respect to the radicals formed by the classical chemical and thermal initiation mechanisms. These are denoted as PRl, P_n and GP_n, for the primary-radicals, the free radicals and the grafted ones, respectively.

Accordingly, the overall inhibition/retardation effect of carbon black is taken into account by considering that its presence will either lead to complete or partial deactivation of primary radicals, as has been observed for different chemical substances that can act as both inhibitors and retarders in a polymerization system [53]. In this sense, the consideration of additional chemical reactions for the deactivation of reduced-activity primary radicals has been considered redundant in terms of its effect on the overall course of the polymerization and has not been included in the kinetic scheme. Note that, the two aforementioned general categories, grafting and catalyzed ini-

tiator decomposition, are not independent of one another as some reactions of the proposed kinetic scheme belong to both of them (e.g., reactions (7) and (29)).

From the above, it becomes obvious that the postulated kinetic scheme displays a general form, allowing the incorporation of different effects and observed phenomena. In the case of the absence of GTR, the kinetic scheme reduces to the typical homopolymerization case. This is taken into account in the proposed model by setting the quantity of GTR equal to zero, without the necessity to modify any other parameter or equation of the model. A global set of kinetic rate constants has been identified and employed for the simulation of all tested cases and conditions, either in the presence of GTR or for the pure homopolymerization system. Two different peroxide initiators have been tested, namely dicumyl peroxide (DCP) and BPO. DCP has been implemented in order to compare the results of the model with reported homopolymerization data [37]. On the other hand, BPO has been shown to display more interesting behavior in terms of its interactions with carbon black and, as such, has been extensively tested by the present model.

To avoid the multiplication of the parameters of the model, the reduced activity of the carbon black-initiated radicals has been taken into account by a correcting coefficient, α. Accordingly, the kinetic rate constant of a chemical reaction containing reduced-activity radicals has been considered equal to the rate constant of the respective reaction of normal-activity radicals, multiplied by α. In the case of reactions between reduced-activity radicals, the respective rate constant has been multiplied by α^2. Details about the parameters of the model are given later in section 4.5. Note also that some

of the postulated chemical reactions have been denoted in a condensed form to avoid redundant repetitions. This is, for example, the case with the termination reactions including grafted and/or reduced-activity radicals, where the combination and disproportionation reactions have been condensed in a single chemical reaction (i.e., Eqs. (28)-(30)).

4. Model developments

On the basis of the postulated general kinetic scheme (i.e., reactions (1)-(40)), the net rates of production of the different species that are present in the reacting mixture can be established. They are divided into the rates of the macromolecular and the non-macromolecular species. The first category includes the free, grafted and reduced-activity radicals as well as the free and grafted polymer chains, while the second category includes all the remaining species, such as initiator agents, styrene, GTR, carbon black, primary radicals, AH adduct and AR and MR radicals. Note that, in this study, GTR has been considered as a non-macromolecular species, despite its macromolecular nature. In fact, in the framework of the present kinetic model, GTR participates in the kinetic developments by its chemical groups that are exposed to the rest of the reacting species and are prone to react. As such, it is not the macromolecular character of the different elastomers, that are present in the formulation of GTR, that constitutes an element of interest for the model, but rather the quantity of these groups. This quantity is denoted in the model equations by G and details on its calculation are given later in the text (see Eq.(65) in section 4.4).

Finally, it should be noted that the present approach is based on the

assumptions of i) chain-length independent rate constants for all the reactions and ii) homogeneous reacting mixture. In fact, the majority of previous modeling studies of the system of rubber-grafting polymerization have treated the system as homogeneous, with some exceptions where a heterogeneous approach was implemented mainly to describe the phase-inversion stage of the formation of HIPS [8, 51]. The consideration of mass transfer and diffusion phenomena within the structure of GTR is expected to provide a more realistic representation of the system, notably at high GTR loading, as well as a more plausible concentration profile of the different species at the grafting sites. However, this would further complicate the model and increase its number of parameters. It would also necessitate accurate relevant measurements that, for the moment, are not reported for this system. In this respect and considering the nature of the systems and the conditions studied in this work, the aforementioned diffusional limitations, beyond the point to which the difference in the kinetic rate constants between grafting and homopolymerization reactions can capture, have been considered negligible.

4.1. Rate functions of the macromolecular species

In this section, the development of the net rate of production of only one macromolecular species is presented, namely that of the free radicals of size 'n', R_n, while the rest of the rate functions are presented in detail in Appendix A:

$$
\begin{aligned}
r_{R_n} = & \left(k_I \cdot [PR] \cdot [M] + k_{fm} \cdot [M] \cdot \sum_{k=1}^{\infty} [R_k] \right) \cdot \delta(n-1) \\
& + k_A \cdot [AR] \cdot [M] \cdot \delta(n-3) + k_B \cdot [MR] \cdot [M] \cdot \delta(n-2) \\
& + k_p \cdot [M] \cdot ([R_{n-1}] - [R_n]) - (k_{fm} \cdot [M] + k_{fAH} \cdot [AH]) \cdot [R_n] \\
& + k_s \cdot [PR] \cdot \sum_{k=n+1}^{\infty} [D_k] - (k_{tc} + k_{td}) \cdot [R_n] \cdot \sum_{k=1}^{\infty} [R_k] \\
& - k_{tPR} \cdot [PR] \cdot [R_n] + \left(k_{fmG} \cdot [M] \cdot \sum_{k=1}^{\infty} [GR_k] \right) \cdot \delta(n-1) \\
& - k_{fG} \cdot [G] \cdot [R_n] + k_{sG} \cdot [PR] \cdot \sum_{k=n+1}^{\infty} [GD_k] \\
& - (k_{tcG} + k_{tdG}) \cdot [R_n] \cdot \sum_{k=1}^{\infty} [GR_k] - k_{dea} \cdot [CB] \cdot [R_n] \\
& - \alpha \cdot [R_n] \cdot \left((k_{tc} + k_{td}) \cdot \sum_{k=1}^{\infty} [P_k] + (k_{tcG} + k_{tdG}) \cdot \sum_{k=1}^{\infty} [GP_k] \right)
\end{aligned}
\tag{41}
$$

In the above equation, the rate of production of R_n, r_{R_n} is expressed in units of molar concentration over time (i.e., $mol.l^{-1}.min^{-1}$), while the molar concentrations of the different species (i.e., in $mol.l^{-1}$) are denoted with the use of brackets [ ]. Also, $\delta(n-1)$ is the Kroenecker's delta, given by:

$$
\delta(n-i) = \begin{cases} 1 & \text{for n = i} \\ 0 & \text{for n} \neq \text{i} \end{cases} \tag{42}
$$

Note that, in the present work, the complete mathematical model was developed in Matlab to allow for a maximum control over the derivation of the model equations (i.e., in contrast to commonly employed polymerization-specific software).

4.2. Method of Moments

Since the rate functions of the macromolecular species (Eq.(41) and Eqs.(A.1)-(A.5)) are described with respect to their chain length, the resulting system of differential equations (see Eqs.(62)-(63)) will be of size equal to the considered maximum chain-length. In this respect, one of the most commonly employed techniques to reduce the size of the system and the associated computational effort is the method of moments [54]. It is a widely-used technique that is based on the statistical representation of the average molecular properties of the macromolecular species in terms of the leading moments of their number-chain-length distribution. Accordingly, one can define the moment of order k, for the free radicals, R_n, as:

$$\lambda_k = \sum_{n=1}^{\infty} n^k R_n \tag{43}$$

The moments for the rest of the macromolecular species can be defined accordingly. Following the above definition, the rate function of the free radicals (Eq.(41)) can be readily transformed to express the rate function of their leading moments:

$$
\begin{aligned}
r_{\lambda_k} &= k_I \cdot [PR] \cdot [M] + k_{fm} \cdot [M] \cdot \lambda_0 \\
&+ 3^k \cdot k_A \cdot [AR] \cdot [M] + 2^k \cdot k_B \cdot [MR] \cdot [M] \\
&+ k_p \cdot [M] \cdot \left(\sum_{r=0}^{k} \binom{k}{r} \lambda_r - \lambda_k \right) - (k_{fm} \cdot [M] + k_{fAH} \cdot [AH]) \cdot \lambda_k \\
&+ k_s \cdot [PR] \cdot T_1 - (k_{tc} + k_{td}) \cdot \lambda_k \cdot \lambda_0 - k_{tPR} \cdot [PR] \cdot \lambda_k \\
&+ k_{fmG} \cdot [M] \cdot \nu_0 - k_{fG} \cdot [G] \cdot \lambda_k + k_{sG} \cdot [PR] \cdot T_{1G} - (k_{tcG} + k_{tdG}) \cdot \lambda_k \cdot \nu_0 \\
&- k_{dea} \cdot [CB] \cdot \lambda_k - \alpha \cdot \lambda_k \cdot ((k_{tc} + k_{td}) \cdot \theta_0 + (k_{tcG} + k_{tdG}) \cdot \omega_0)
\end{aligned}
\tag{44}
$$

In the above expression, $\binom{k}{r}$ denotes the binomial coefficients and T_1 and T_{1G} are given by:

$$
T_1 = \sum_{m=0}^{k} \frac{B_m}{k-m+1} \left(\mu_{k-m+1} - \mu_0 \right) \qquad ; \qquad T_{1G} = \sum_{m=0}^{k} \frac{B_m}{k-m+1} \left(\xi_{k-m+1} - \xi_0 \right)
\tag{45}
$$

with the Bernoulli numbers defined as:

$$
B = \left[1, \ -\frac{1}{2}, \ \frac{1}{6}, \ 0, ... \right]
\tag{46}
$$

In these expressions, ν_k, ξ_k, θ_k and ω_k denote respectively the moments of GR_n, GD_n, P_n and GP_n. The notation of all the different moment species is defined in the Nomenclature section and the corresponding rate functions are detailed in Appendix A (Eqs.(A.6)-(A.10)).

4.3. Rate functions of the non-macromolecular species

The net production rates of the non-macromolecular species of interest can be defined on the basis of their participation in the different chemical reactions of the postulated general kinetic scheme (Eqs.(1)-(40)):

- Styrene monomer, M

$$\begin{aligned} r_M = & -\left(k_I \cdot [PR] + (k_p + k_{fM}) \cdot \lambda_0\right) \cdot [M] \\ & -\left((k_2 + k_C) \cdot [AH] + k_A \cdot [AR] + k_B \cdot [MR]\right) \cdot [M] \\ & -\left(k_{pG} \cdot ([GPR] + \nu_0) + k_{fmG} \cdot \nu_0\right) \cdot [M] \\ & - 2 \cdot k_1 \cdot [M]^2 + 2 \cdot k_{-1} \cdot [AH] - \alpha \cdot k_I \cdot [PRl] \cdot [M] \\ & - \alpha \cdot (k_p \cdot \theta_0 + k_{pG} \cdot \omega_0) \cdot [M] \end{aligned} \tag{47}$$

- Ground Tire Rubber, G

$$r_G = -\left(k_{IG} \cdot ([PR] + \alpha \cdot \ [PRl]) + k_{fG} \cdot \lambda_0\right) \cdot [G] \tag{48}$$

- Carbon Black, CB

$$\begin{aligned} r_{CB} = & -\left(k_{dCB} \cdot [I] + k_{dea} \cdot (\lambda_0 + \alpha \cdot \theta_0) + k_{deaG} \cdot (\nu_0 + \alpha \cdot \omega_0)\right) \cdot [CB] \\ & - k_{dea} \cdot ([PR] + [GPR] + [AR] + [MR]) \cdot [CB] \end{aligned} \tag{49}$$

- Initiator, I

$$r_I = -\left(k_d + k_{dCB} \cdot [CB]\right) \cdot [I] \tag{50}$$

- Diels-Alder adduct, AH

$$\begin{aligned} r_{AH} = & \ k_1 \cdot [M]^2 - \left(k_{-1} + (k_2 + k_C) \cdot [M]\right) \cdot [AH] \\ & -\left(k_{fAH} \cdot \lambda_0 + k_{fAHG} \cdot \nu_0\right) \cdot [AH] \end{aligned} \tag{51}$$

- Styryl radicals, MR

$$r_{MR} = k_2 \cdot [AH] \cdot [M] - k_B \cdot [M] \cdot [MR] - k_{dea} \cdot [MR] \cdot [CB] \tag{52}$$

- 1-Phenyl tetraryl radicals, AR

$$\begin{aligned} r_{MR} = {} & k_i \cdot [AH] \cdot [M] - k_A \cdot [M] \cdot [AR] \\ & + (k_{fA} \cdot \lambda_0 + k_{fAG} \cdot \nu_0) \cdot [AH] - k_{dea} \cdot [AR] \cdot [CB] \end{aligned} \tag{53}$$

- Primary radicals, PR

$$\begin{aligned} r_{PR} = {} & 2 \cdot f_1 \cdot k_d \cdot [I] - k_I \cdot [M] \cdot [PR] \\ & - k_{IG} \cdot [G] \cdot [PR] - (k_s \cdot \mu_0 + k_{sG} \cdot \xi_0) \cdot [PR] \\ & - (k_{tPR} \cdot \lambda_0 + k_{tPRG} \cdot \nu_0 + k_{dea} \cdot [CB]) \cdot [PR] \end{aligned} \tag{54}$$

- Grafted primary radicals, GPR

$$\begin{aligned} r_{GPR} = {} & k_{IG} \cdot [G] \cdot [PR] - k_{pG} \cdot [M] \cdot [GPR] + k_{fG} \cdot [G] \cdot \lambda_0 \\ & - k_{dea} \cdot [CB] \cdot [GPR] \end{aligned} \tag{55}$$

- Reduced-activity primary radicals, PRl

$$r_{PRl} = f_2 \cdot k_{dCB} \cdot [CB] \cdot [I] - \alpha \cdot (k_I \cdot [M] + k_{IG} \cdot [G]) \cdot [PRl] \tag{56}$$

- Deactivated primary radicals, DPR

$$r_{DPR} = k_{dea} \cdot [CB] \cdot ([PR] + [GPR]) \tag{57}$$

It should be noted that the deactivated primary radicals, DPR, are not consumed in any reaction and, thus, the rate function of their concentration (Eq.(57)) serves only in the overall mass balance check. For the calculation

of the evolution of the concentration of the different primary radical species (i.e., PR, GPR and PRl), as well as for the Diels-Alder adduct, AH, the quasi-steady-state assumption (Q.S.S.A.) has been employed, leading to the following expressions:

- Diels-Alder adduct, AH

$$[AH] = \frac{k_1 \cdot [M]^2}{k_{-1} + (k_i + k_C) \cdot [M] + k_{fAH} \cdot \lambda_0 + k_{fAHG} \cdot \nu_0} \tag{58}$$

- Primary radicals, PR

$$[PR] = \frac{2 \cdot f_1 \cdot k_d \cdot [I]}{k_I \cdot [M] + k_{IG} \cdot [G] + k_s \cdot \mu_0 + k_{sG} \cdot \xi_0 + k_{tPR} \cdot \lambda_0 + k_{tPRG} \cdot \nu_0 + k_{dea} \cdot [CB]} \tag{59}$$

- Grafted primary radicals, GPR

$$[GPR] = \frac{k_{IG} \cdot [G] \cdot [PR] + k_{fG} \cdot [G] \cdot \lambda_0}{k_{pG} \cdot [M] + k_{dea} \cdot [CB]} \tag{60}$$

- Reduced-activity primary radicals, PRl

$$[PRl] = \frac{f_2 \cdot k_{dCB} \cdot [CB] \cdot [I]}{\alpha \cdot (k_I \cdot [M] + k_{IG} \cdot [G])} \tag{61}$$

4.4. Reactor design equations

The reactor design equations, for a batch polymerization system, can be directly derived for all the species of interest (i.e., non-macromolecular species and leading moments of the macromolecular species), on the basis of the established rate functions. In this respect, the resulting system of ordinary differential equations (ODEs) will be of the form:

$$\frac{dn_S}{dt} = r_S \cdot V \tag{62}$$

where S denotes the different species of interest and V is the volume of the reacting mixture, which also varies according to:

$$\frac{dV}{dt} = r_M \cdot \left(\frac{1}{d_M} - \frac{1}{d_P}\right) \cdot M_0 \cdot V \tag{63}$$

where M_0 is the molecular weight of styrene and d_M and d_P are the respective densities of styrene and polystyrene in $g.mol^{-1}$, calculated by the following expressions [37]:

$$d_m = 9.236 \cdot 10^{-1} - 0.887 \cdot T(^{\circ}C) \qquad ; \qquad d_p = 1.085 - 0.605 \cdot T(^{\circ}C) \tag{64}$$

The above system of ODEs is completed by the algebraic equations for the calculation of the concentrations of AH, PR, GPR and PRl (Eqs.(58)-(61)). This system of ODEs was numerically solved using a variable step and variable order numerical integration method, as implemented in the function "ode15s" of the toolbox of Matlab, which is specifically adapted for stiff systems. For the determination of the initial concentration of G, corresponding to the available reaction sites on the accessible internal and external surface of the GTR particles, the following approach has been adopted: the composition of GTR, in terms of the type and weight fraction of elastomers, as provided by the supplier, has been considered in order to calculate a theoretical estimation of the molar quantity of double bonds. This quantity has also been found to coincide with the experimental determination of the concentration of double bonds of the elastomer chains of GTR, which was

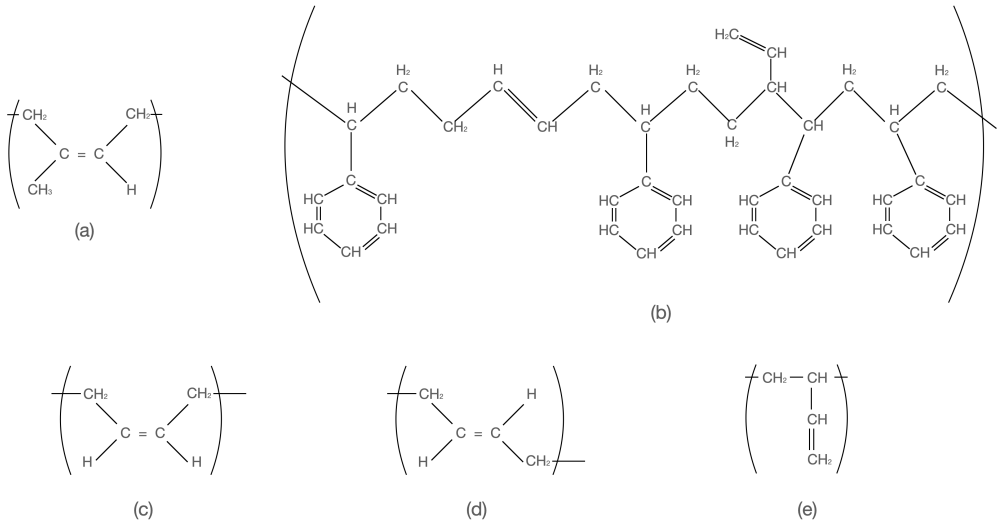

Scheme 2: Chemical structure of (a)*cis*-Polysioprene, (b)Styrene-Butadiene Rubber, (c)*cis*-1,4-Polybutadiene, (d)*trans*-1,4-Polybutadiene, (c)Vinyl-1,2-polybutadiene.

carried out according to the standard test method for iodine value of drying oils and fatty acids (ASTM D-1959). Both experimental and theoretical values were found to be of the order of $3.5 \cdot 10^{-3}$ mol of double bonds per gram of GTR. The composition of GTR is shown in Table 1 while the chemical structures of the most commonly encountered elastomers in GTR are given in Scheme 2. The calculated value of double bonds was multiplied by an efficiency factor in the model (i.e., parameter f_{GTR}, whose value was set to 0.53 - see Table2) to transform it to available reaction sites, prone to react. Finally, to account for the exposure and coverage of these possible reaction sites on GTR, the initial concentration of G was calculated according to the following expression:

$$[G]_0 = \frac{\left(\frac{GRat}{GRat_c}\right)^6}{1+\left(\frac{GRat}{GRat_c}\right)^6} \cdot [M_{DB}] \cdot f_{GTR} \qquad ; \qquad GRat = \frac{W_{GTR}}{W_{GTR}+W_{St}} \quad (65)$$

In the above expression, $Grat$ and $Grat_c$ denote the actual mass fraction of GTR in the mixture and a critical value of this mass fraction, respectively ($Grat_c = 0.43$ - see Table 2). M_{DB} is the calculated molar concentration of double bonds of GTR according to the procedure described previously.

According to the relative literature, there exist two principal mechanisms for the grafting reactions, namely the addition of radicals to the unsaturated double bonds of the elastomers of GTR and the mechanism of hydrogen abstraction by the radicals [4, 11, 12, 41, 55, 42]. The extent to which grafting by any of these two mechanisms will take place is primarily dictated by the type of radicals and elastomers as well as by the position of the double bonds (i.e., as pendant side-chain groups or within the main backbone of the elastomer, see also Scheme 2). The same factors affect also the competition between homopolymerization and grafting reactions. In this respect, and given that GTR is composed of a mixture of different elastomers, as shown in Table 1, the calculation, in the model, of the quantity of sites of GTR that are prone to participate in grafting reactions has been based on the above simplified and generalized approach. Thus, the initial calculation of the amount of double bonds of GTR allows the consideration of the actual composition and characteristics of GTR, while the implementation of the parameter f_{GTR} provides a degree of liberty and includes the aforementioned variations. In addition, the first term of Eq.(65) was introduced to account

Table 1: Formulation of GTR.

Elastomer	Weigh fraction
Styrene-butadiene rubber	0.4
Polyisoprene	0.3
Polybutadiene	0.2
Butadiene-acrylonitrile rubber	0.05
Isobutylene-isoprene rubber	0.05

for the coverage and masking effects that have been observed for different GTR contents [23]. In fact, the sigmoidal curve, resulting from the application of Eq.(65), allows for the consideration of a critical GTR concentration, beyond which the observed effects are gradually attenuated. As such, any mathematical expression resulting in similar functional forms could provide similar results. The previous experimental study of Florez et al. [23] has shown that this critical concentration should be below 50% of GTR and the parametric estimation of the model proposed in this work has resulted in a value equal to 0.43 for this parameter, as shown in Table 2, which is in accordance with the previous findings. Finally, the initial concentration of carbon black, in the model, was considered equal to a fixed percentage of $[G]_0$, set to 30% in this study.

4.5. Kinetic rate constants

The values of the model parameters were estimated in a two-step process, on the basis of reported values (when available). More specifically, in the first step, the kinetic rate constants of the reactions corresponding only to the pure homopolymerization case (i.e., in the absence of GTR) were estimated on the

basis of the available homopolymerization data. Among them, the values of $k_{d,DCP}$, $k_{d,BPO}$, k_{-1}, k_1/k_{-1}, k_2 and k_{tc} were taken directly from the relevant literature [37, 56], as shown in Table 2. The values of k_p, k_C, k_{fAH} and k_{fm}, were tuned via the implementation of the Nedler-Mead optimization algorithm of Lagarias et al. [57], from the optimization toolbox of Matlab, using all the available homopolymerization data, presented in this work (see Figures 1-4). This concerned both pre-exponential factors and activation energies, simultaneously. The values of these parameters were then kept constant throughout the rest of the estimation process. In addition to the parameters defined in Table 2, the commonly adopted assumption of $k_A = k_B = k_I = k_p$ has been adopted.

The second step of the estimation process concerned only the model parameters of the reactions related to the presence of GTR in the system. However, given the fact that, in the framework of this work, the only relevant available data concerned the temporal evolution of monomer conversion, the proposed kinetic model has been reduced accordingly. In this respect, only the chemical reactions of the proposed general kinetic scheme that are directly associated with the evolution of monomer conversion, in the presence of GTR, were considered in the parametric estimation process (see Table 2). The kinetic rate constants of the rest of the reactions involving GTR and carbon-black were set to zero. In fact, it would be meaningless to attempt to estimate at this point the complete set of rate constants solely on the basis of monomer conversion measurements. A new study has been launched aiming to acquire additional experimental data on molar mass and grafting efficiency indexes, which will allow the estimation of all the kinetic constants of the

model. Until then, and in the absence of relevant data in the literature, the present work aims to demonstrate that the proposed unified modeling framework is capable of predicting the behavior of the system, as observed through the currently available data, both in the absence and in the presence of GTR. In addition, it presents a general kinetic scheme that can be implemented for the modeling of other polymerization systems in the presence of GTR. The final reduced form of the kinetic scheme, corresponding to the retained chemical reactions in this study, is presented in Appendix B.

Accordingly, the parameters presented in Table 2, besides the previously estimated ones on the basis of the homopolymerization data, were estimated via the Nedler-Mead algorithm using the DSC data of Florez et al. [23]. More particularly, an initial set of values was estimated on the basis of the DSC data at 90°C and then another one at 120°C. From the values of the parameters obtained for the two above temperatures, the pre-exponential factor and the activation energy of k_{dCB}, as well as the linear correlation parameters (i.e., with respect to temperature) of k_{pG}/k_p and k_{IG}/k_p were determined via linear regression. On the other hand, the values of k_{tcG}/k_{tc}, k_{dea}/k_p and k_{deaG}/k_{dea} were kept fixed, as they did not display significant variation with temperature. Finally, all the parameters, related to the copolymerization system, were fine-tuned to their final values in an ultimate optimization step using all available DSC data (i.e., at 85°C, 90°C and 120°C). Note that, the implementation of rate constant ratios for the reactions involving GTR over their homopolymerization counterparts was made in an attempt to constrain the number of parameters of the model.

Table 2: Model parameters

Parameter	Value	Units	Reference
$k_{d,DCP}$	$5.500 \cdot 10^{17} \cdot exp(-36650/R/T)$	min^{-1}	[37]
$k_{d,BPO}$	$2.289 \cdot 10^{14} \cdot exp(-27233/R/T)$	min^{-1}	[56]
k_p	$1.149 \cdot 10^{9} \cdot exp(-7513/R/T)$	$l.mol^{-1}.min^{-1}$	This work
k_{-1}	$6.840 \cdot 10^{3} \cdot exp(-13533/R/T)$	min^{-1}	[37]
k_1/k_{-1}	$6.400 \cdot 10^{4} \cdot exp(-12907/R/T)$	$l.mol^{-1}$	[37]
k_2	$9.800 \cdot 10^{7} \cdot exp(-23883/R/T)$	$l.mol^{-1}.min^{-1}$	[37]
k_C	$2.360 \cdot 10^{6} \cdot exp(-21346/R/T)$	$l.mol^{-1}.min^{-1}$	This work
k_{fm}	$1.032 \cdot 10^{7} \cdot exp(-10545/R/T)$	$l.mol^{-1}.min^{-1}$	This work
k_{fAH}	$7.360 \cdot 10^{7} \cdot exp(-30800/R/T)$	$l.mol^{-1}.min^{-1}$	This work
k_{tc}	$7.530 \cdot 10^{10} \cdot exp(-1677/R/T)$	$l.mol^{-1}.min^{-1}$	[37]
k_{dCB}	$2.147 \cdot 10^{-1} \cdot exp(-1478.7/R/T)$	$l.mol^{-1}.min^{-1}$	This work
$log(k_{pG}/k_p)$	$5.34 \cdot 10^{-2} \cdot T(^{\circ}C) - 5.1574$	-	This work
$log(k_{IG}/k_p)$	$7.52 \cdot 10^{-2} \cdot T(^{\circ}C) - 7.1353$	-	This work
k_{tcG}/k_{tc}	9.823	-	This work
k_{dea}/k_p	0.310	-	This work
k_{deaG}/k_{dea}	3.770	-	This work
α	$3.70 \cdot 10^{-6}$	-	This work
f_1	0.65 (0.83 for DSC data)	-	This work
f_2	0.40	-	This work
f_{GTR}	0.53	-	This work
$GRat_c$	0.43	-	This work
$a_m; a_p$	$1.4 \cdot 10^{-3}; 4.8 \cdot 10^{-4}$	K^{-1}; K^{-1}	[39], this work
$\delta; \sigma$	$3.8 \cdot 10^{-9}; 3.7 \cdot 10^{-9}$	$m; m$	This work
$j_c; \delta_c$	$175; 5.0 \cdot 10^{-4}$	$-; l.g^{-1}$	[39], this work
$A_{cr}; E_{cr}/R$	$9.0; 1960^{32}$	$g^{1/2}.mol^{-1/2}; K$	This work
$A_{crm}; E_{crm}$	$0.231; 1670$	$-; cal.mol^{-1}$	[39], this work
$A; B; C/B; n$	$0.4315; 0.7; 0.9; 2.5$	$-; -; -; -$	This work

$R = 1.9872\ cal.mol^{-1}.K^{-1}$

The final set of estimated parameter values, as presented in Table 2, has been kept constant and unchanged for all the simulations presented in this work, both in the absence and in the presence of GTR. However, the efficiency factor of the initiator decomposition (Eq.(1)), f_1, was set to a higher value for the simulations of the DSC data, in order to compensate the expected differences between the experimental systems in terms of the level of impurities and homogeneity (see Table 2). Finally, some rate constants of reactions related to the pure homopolymerization case (e.g., termination by disproportionation, Eq.(25), termination by primary radicals, Eq.(32), as well as scission reactions, Eq.(22), which are expected to have an impact only when the polymerization is kept to relatively high temperatures for long periods of time [39]), were also set to zero, in accordance with reported studies and/or with the generated data. The same was done for their copolymerization counterparts. These parameters are not reported in Table 2.

The proposed model also takes into account the diffusion controlled phenomena affecting the reactions of termination, propagation and initiation, also known as the gel-, glass- and cage-effects, respectively. To this end, the model originally proposed by Marten and Hamielec [32] was employed. The equations of this model are omitted here but can be found in the original study, as well in more recent studies that have adopted it [39], while the values of its parameters are given in Table 2. Note that, the model of Marten and Hamielec [32] was adopted in its complete form, including all the above diffusion-controlled phenomena, for the sake of completeness and generality in the applicability of the presented kinetic model. It is worth noting at this point that the choice of the diffusional model largely affects the parametric

estimation process and, as such, the final values of the kinetic constants of the model, as shown in D'hooge et al. [58]. Alternative diffusional models for the polystyrene system can also be found in the reported literature [33, 59].

5. Model results and discussion

The model has been initially validated against reported data for the pure styrene hopolymerization system, in the absence of GTR. Different data sources and polymerization conditions have been tested to assure its generality and robustness. Monomer conversion and average molecular weight predictions have been compared to their respective experimental data, either as specific point predictions or as complete temporal evolution profiles, depending on the availability of the data. In all presented cases, the predictions of the model are plotted as curves and the experimental data as discrete points.

In this respect, Figure 1 compares the experimental data for the temporal evolution of monomer conversion and average molecular weights, reported in Villalobos et al. [56], with the respective predictions of the model. It is seen that the model succeeds in following with great accuracy the evolution of all three experimental data sets. Note that the same set of data has also been used previously as reference for the validity of other reported models [39].

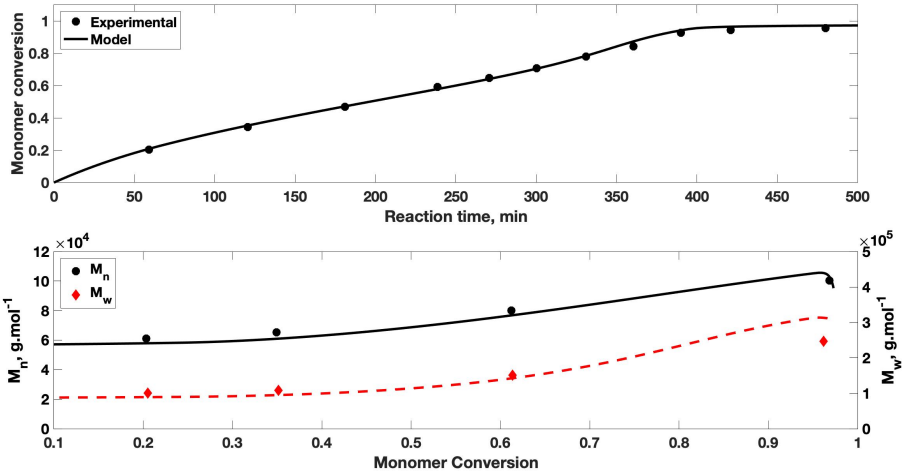

Figure 1: Comparison between model predictions and reported experimental data [56]; upper figure: time evolution of monomer conversion; lower figure: time evolution of number-average (left y axis, filled circles and solid curve) and weight-average (right y axis, filled diamonds and dashed curve) molecular weights. (T = 90 °C; BPO 0.01 $mol.l^{-1}$; $f_1 = 0.65$).

Similarly, another set of data that can be used as a reference point, is the one presented in the work of Kotoulas et al. [37], as it covers a wide range of temperatures and, thus, incorporates the significance of the thermal initiation mechanism. The comparison of these data, for four different reaction temperatures (i.e., from 120 °C to 150°C), with the respective predictions of the model developed in this work, are shown in Figure 2. As can be seen, the model succeeds in following with high accuracy all the monomer conversion time-histories as well as the molecular weights at the highest temperatures, but under-predicts the average molecular weights at high monomer conversions, notably for temperatures $\leq$ 130 °C. The observed disagreement may be related to the incapacity of the employed gel-effect model to accu-

rately describe the related phenomena, as also evidenced by the fact that this disagreement is principally located in the conversion range where diffusion-controlled phenomena become very important, marked by the characteristic s-shape of the curves at these temperatures. In fact, in the original work of Kotoulas et al. [37], a more comprehensive model has been employed for the description of the diffusion-controlled phenomena [33], instead of the one selected here [32]. In any case, the selected gel-effect model was considered to be sufficient to describe the observed behavior of the rest of the tested data.

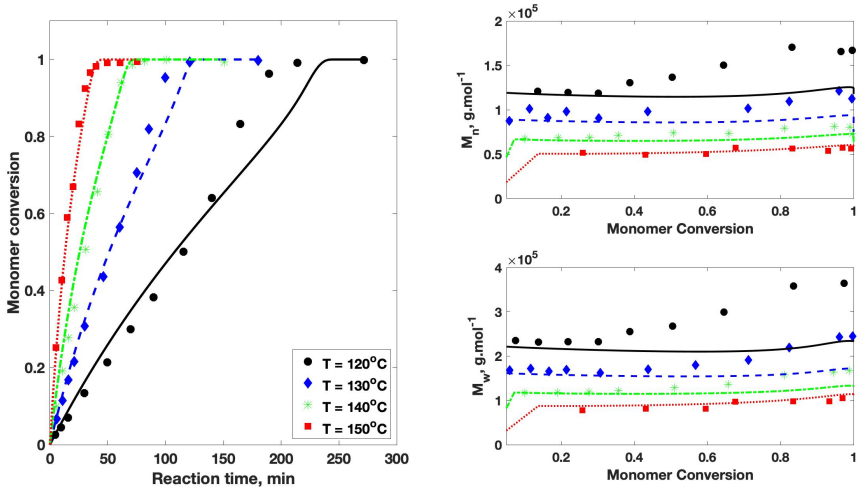

Figure 2: Comparison between model predictions and reported experimental data for different reaction temperatures [37]; left figure: time evolution of monomer conversion; upper right figure: evolution of number-average molecular weight with respect to the monomer conversion; lower right figure: evolution of weight-average molecular weight with respect to the monomer conversion. (Filled circles and solid curves: T= 120 °C; filled diamonds and dashed curves: T= 130 °C; stars and dash/point curves: T= 140 °C; filled squares and point curves: T= 150 °C; DCP 4000 ppm; $f_1 = 0.65$).

The model has also been tested on solution polymerization experiments, carried out in a bench-scale reactor, as described in Section 2.2. These experiments were realized within the framework of a study that was focused on the final average molecular weight of the produced polystyrene [26]. As such, not enough intermediate data were recorded to allow the tracking of the complete temporal evolution of the course of the polymerization. Nonetheless, the comparison with the model predictions, depicted in Figure 3, provides evidence that the model remains coherent in this solution polymerization case as well, under two different polymerization temperatures.

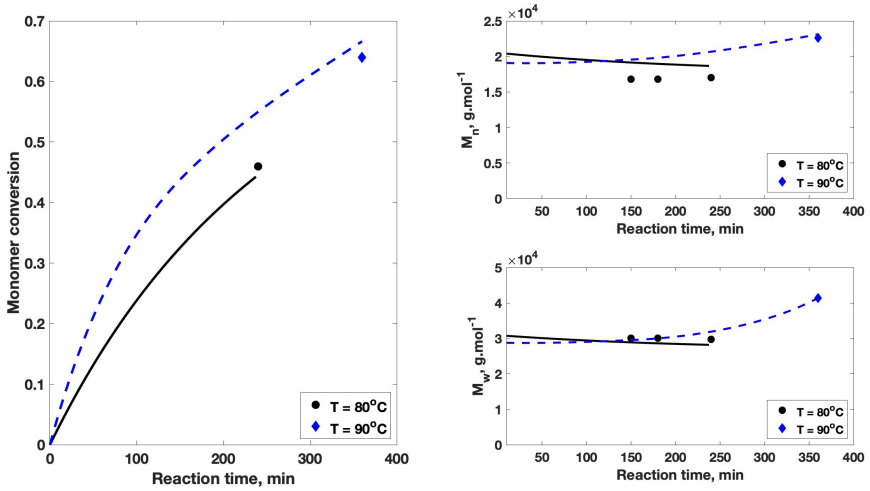

Figure 3: Comparison between model predictions and experimental data of a solution polymerization system [26]; left figure: time evolution of monomer conversion; upper right figure: time evolution of number-average molecular weight; lower right figure: time evolution of weight-average molecular weight. (Filled circles and solid curves: T= 80 °C, BPO 0.54 $\%wt$; filled diamonds and dashed curves: T= 90 °C, BPO 0.36 $\%wt$; $f_1 = 0.65$).

The last set of data of pure styrene homopolymerization, on which the

model has been tested, is the DSC data set that has been produced and reported in the framework of our previous study [23]. This comparison is shown in Figure 4, where the conversion-time histories are plotted for three different reaction temperatures, namely at 85 °C, 90 °C and 120 °C. In all three cases, the model succeeds in tracking both the initial stages of the reaction as well as the onset of the gel- and glass-effect stages that are clearly distinct on the curves of the two lowest reaction temperatures (i.e., marked by the characteristic S-shape of the curves).

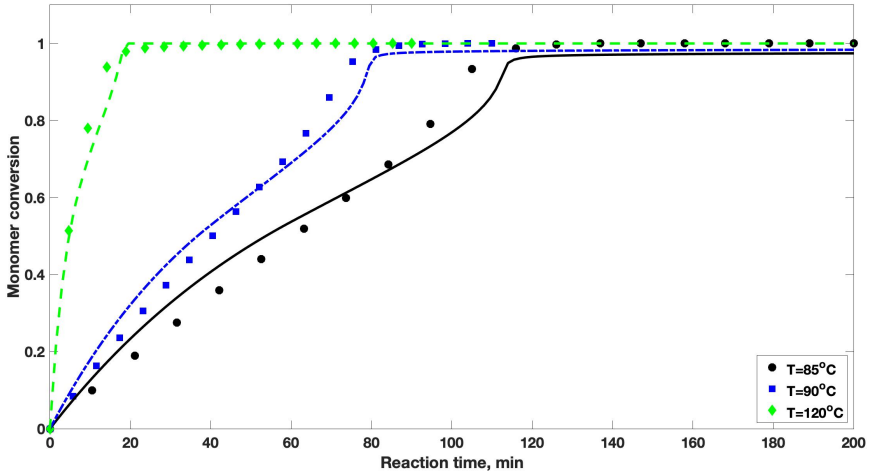

Figure 4: Comparison between model predictions and experimental DSC data of the homopolymerization system [23]. (filled circles and solid curves: T= 85 °C; filled squares and dot/dashed curves: T= 90 °C; filled diamonds and dashed curves: T= 120 °C; BPO/St 4.6 $\%wt$).

Subsequently, the model has been calibrated and tested over a range of DSC data, all produced in the framework of the previously reported experimental DSC study of Florez et al. [23], in the presence of GTR. The first

comparison, shown in Figure 5, concerns the evolution of monomer conversion under different GTR contents and for a given ratio of BPO initiator to styrene. The case of a pure homopolymerization, under the same initiator content, is also included to demonstrate the effect of GTR content on the course of the polymerization. All cases are isothermal at 90 °C. The observed effects of accelerated reaction during the first stage of the polymerization, which is particularly evident in the case of 30% GTR content, and the overall inhibition, in terms of the final monomer conversion, that is proportional to the content of GTR, are both well-captured by the model and coherent to the experimental data. This is due to the inclusion, in the adopted general kinetic scheme, of the reactions of accelerated decomposition of BPO for the production of radicals of reduced activity (Eq.(2)) and the reactions of deactivation of the radicals (Eqs.(34)-(40)), induced by carbon black [23].

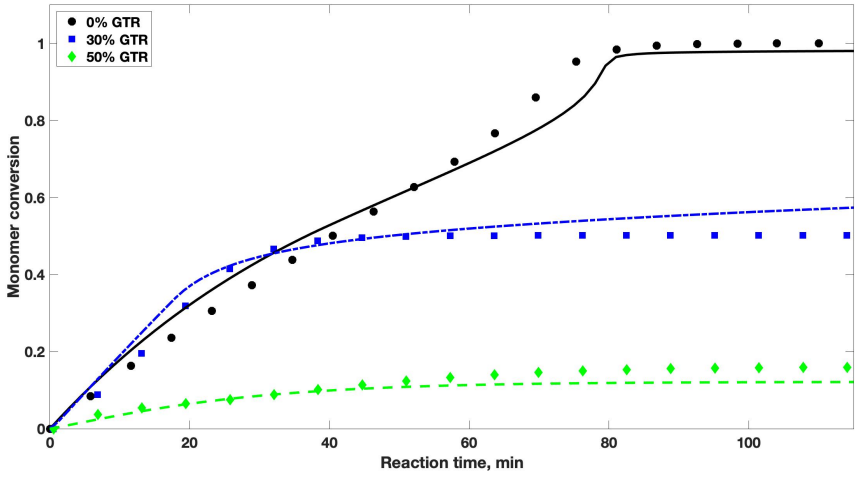

Figure 5: Effect of the GTR content on the evolution of monomer conversion, during the isothermal BPO-initiated polymerization of styrene in the presence of GTR particles [26]. (Filled circles and solid curves: pure homopolymerization; filled squares and dot/dashed curves: 30% GTR; filled diamonds and dashed curves: 50% GTR; T= 90 °C; BPO/St 4.6 $\%wt$).

In Figure 6, the evolution of styrene conversion is plotted for two different initiator contents at a given GTR content of 50%. The respective homopolymer case is also shown on the same plot, to emphasize the difference between the effect of GTR content and that of initiator content on the course of the polymerization. In fact, it is seen that, even a very significant increase of the BPO content, from 4.6% to 9.6%, with respect to the mass of styrene, has a minor positive impact on the evolution and final value of monomer conversion, in comparison to the inhibition induced by the presence of GTR in the mixture. In all cases, the proposed model predicts these effects with very good accuracy.

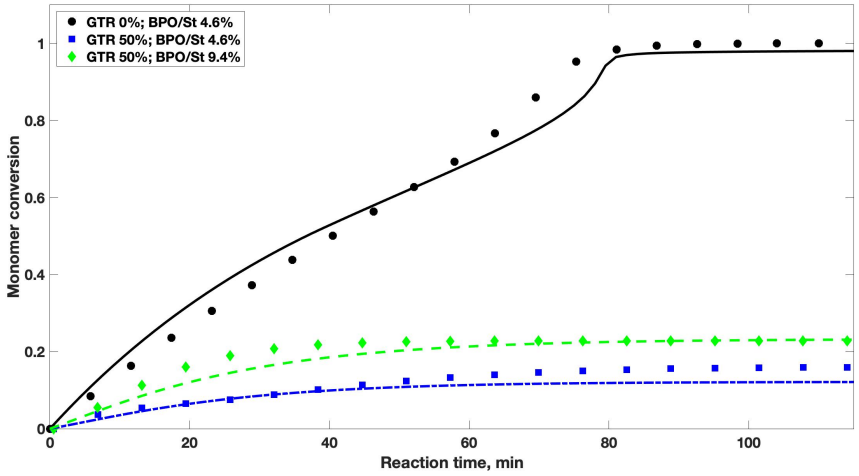

Figure 6: Effect of the initiator content on the evolution of monomer conversion, during the isothermal BPO-initiated polymerization of styrene in the presence of GTR particles [26]. (Filled circles and solid curves: BPO/St 4.6 $\%wt$ with 0% GTR; filled squares and dot/dashed curves: BPO/St 4.6 $\%wt$ with 50% GTR; filled diamonds and dashed curves: BPO/St 9.4 $\%wt$ for 50% GTR; T= 90 °C).

In an attempt to clarify the observed inhibition, the developed model was employed to generate the evolution of additional indicators with time, under the same conditions. Accordingly, the temporal trajectories of monomer conversion, BPO quantity, total radical concentration and ratio of reduced-activity primary radical generation by the decomposition of BPO are shown in Figures (7) and (8). More precisely, Figure (7) shows, on the left, the evolution of monomer conversion for the three copolymer cases of GTR and BPO contents that have been presented previously in Figures (6) and (5), but for longer simulation times than the experimental ones. On the right, the respective evolution of the initiator content is presented for the same cases. From these plots, it becomes evident that, at high GTR content of 50%, the

monomer conversion becomes quickly limited by the rapid consumption of the peroxide initiator, while at a lower GTR content of 30%, the consumption of BPO is significantly slower allowing the system to reach higher values of monomer conversion, which is limited asymptotically at ∼60%, after 800 minutes of reaction.

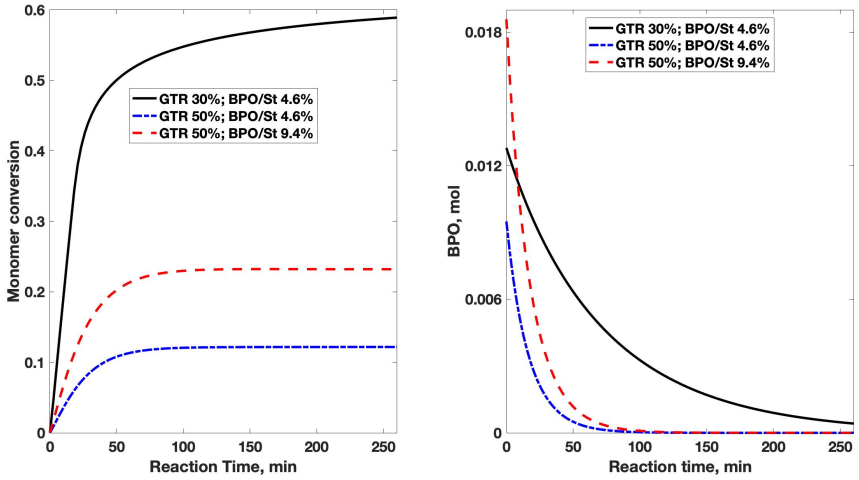

Figure 7: Evolution of monomer conversion (left figure) and BPO content (right figure) with reaction time, for different initial content of GTR and BPO. (Solid curves: BPO/St 4.6 %wt with 30% GTR; dashed curves: BPO/St 4.6 %wt with 50% GTR; dotted curves: BPO/St 9.4 %wt for 50% GTR; T= 90 °C).

Figure (8), shows, on the left, the temporal variation of the total radical quantity (i.e., $\lambda_0+\nu_0+\theta_0+\omega_0$) for the same cases. The observed peaks, which are typical of radical polymerization systems, are completely consistent with the monomer conversion trajectories, since the two cases corresponding to the higher GTR content display more pronounced peaks, that are narrower and are positioned earlier than the 30% GTR case. At the same time, between

the two cases of 50% GTR content, the one with the higher initial BPO content displays a taller and broader peak, thus explaining the achievement of higher monomer conversion than the respective case of equal GTR content but lower BPO initial concentration. This is due to the fact that, in the case of 9.4% BPO content, the polymerization takes place at a higher rate, as evidenced by the height of the respective peak, and for longer reaction time, as evidenced by the larger width of the same peak, as well as by the respective BPO consumption curve (see right Fig.(7)). Finally, the right Figure (8) plots the evolution of the fraction of the reduced-activity primary radicals over the total amount of radicals produced by the decomposition of BPO (see Eqs.(34) and (35)). It is seen that, in both cases of 50% GTR content, the production of reduced-activity primary radicals is favored over the production of normal primary-radicals (i.e., the ratio is constantly higher than 0.5), which is consistent with the observed inhibition. At the same time, the higher BPO content slightly favors the normal-activity radicals, which is again pertinent with the higher monomer conversion achieved. On the other hand, in the 30% GTR content case, the reactions proceed with a very low percentage of reduced-activity radicals, due to the low GTR content, thus leading to higher polymerization rate and monomer conversion.

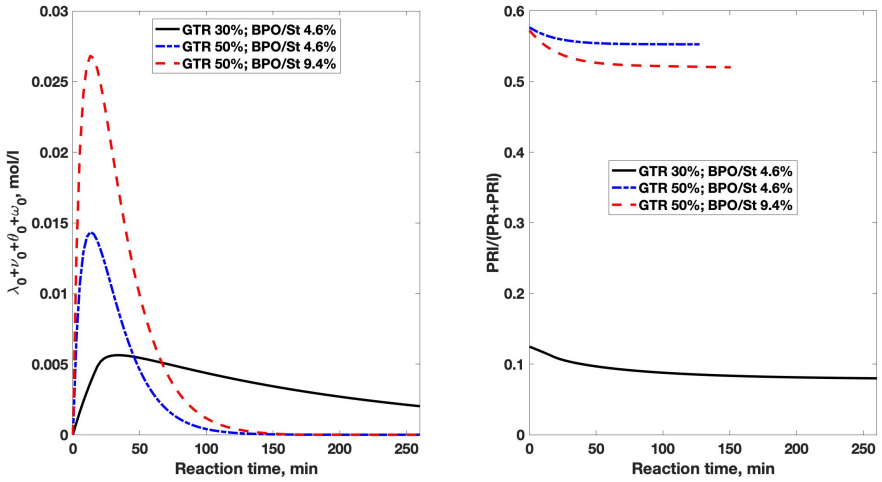

Figure 8: left figure: Evolution of the total quantity of radicals in the system with reaction time, for different initial contents of GTR and BPO; right figure: Temporal evolution of the fraction of reduced-activity primary radicals, produced by the decomposition of BPO, for different initial contents of GTR and BPO. (Solid curves: BPO/St 4.6 %wt with 30% GTR; dashed curves: BPO/St 4.6 %wt with 50% GTR; dotted curves: BPO/St 9.4 %wt for 50% GTR; T= 90 °C).

To further investigate the effect of GTR content on the evolution of the polymerization, a series of simulations were carried out for varying GTR content, at conditions different than the realized DSC experiments. Figure 9 shows the effect of the initial GTR content on the final values (i.e., after 120 min of reaction) of four different quantities, namely the monomer conversion, number average molecular weight, M_n, of the free and the grafted polymer and grafting efficiency. The overall trend of the final monomer conversion is pertinent to the previous observations since it gradually decreases with increasing initial GTR content, as shown in the top Figure. The same behavior is observed for M_n of the free polymer, which seems to gradually

decrease in parallel to the monomer conversion, as one would expect. At the same time, the grafting efficiency, defined as the ratio of the mass of grafted polymer over the total mass of polymer formed in the system, displays an inverse effect of gradual increase along with the increase of the initial GTR content, as shown in the bottom Figure. However, the final number average molecular weight of the formed grafted polymer seems to be unaffected by the initial GTR content, keeping a relatively constant value close to the respective value of the free polymer, as shown by the ratio of the final M_n of the grafted polymer over that of the free polymer, plotted on the right y-axis of the middle Figure. All these effects show that, as the initial amount of GTR increases, GTR-participating reactions are clearly favored in the system, leading to increased inhibition that lowers the monomer conversion and the free polymer molecular weight. At the same time, the grafting reactions are favored thus leading to the formation of more active sites on the particles of GTR and to a higher grafting efficiency. Nonetheless, although the ratio of the grafted polymer radicals over the free ones increases proportionally to the initial GTR content, their rate of polymerization remains comparable in this temperature, as a result of the respective propagation and termination rates. In this sense, free and grafted polymer chains will grow to reach comparative average chain lengths in this temperature, even though their relative population might vary significantly with the initial GTR content. Note that the conditions of the simulations presented in this figure have been selected in order to have a maximum coverage of the monomer conversion and grafting efficiency domains.

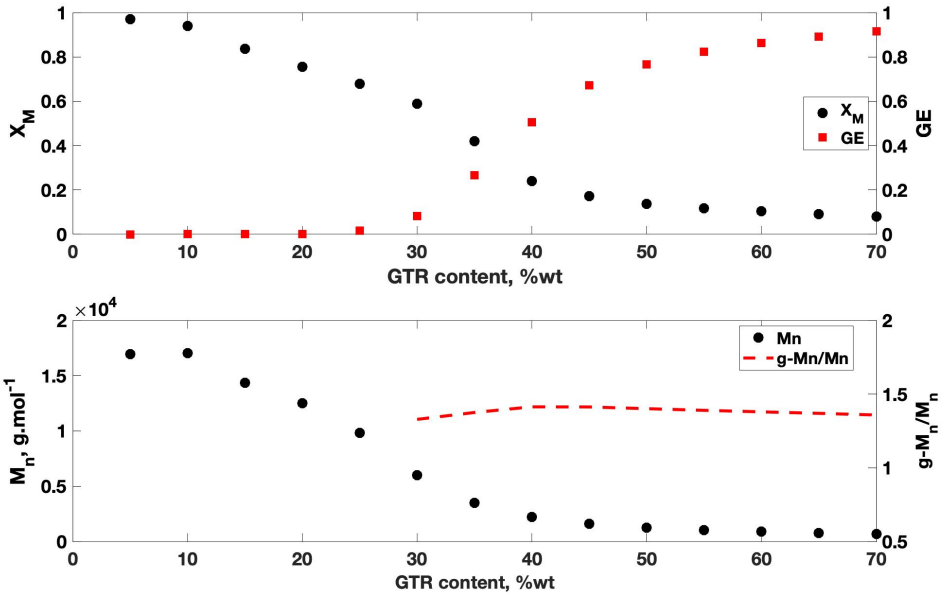

Figure 9: top figure: Effect of the initial GTR content on final monomer conversion (filled black circles, left y axis) and on the final grafting efficiency (filled red squares, right y axis); bottom figure: effect of the initial GTR content on the final number average molecular weight of the free polymer (filled black circles, left y axis) and on the ratio of the final number average molecular weight of the grafted polymer over that of the free polymer (dashed red line, right y axis). (BPO/St 8 $\%wt$; T= 110 °C; reaction time = 120 min).

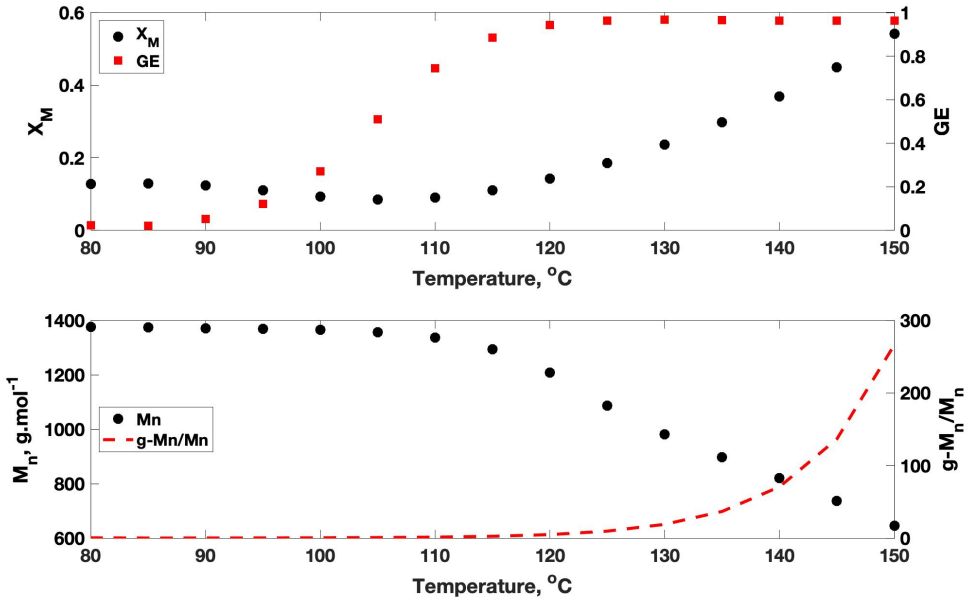

Figure 10: top figure: Effect of the reaction temperature on final monomer conversion (filled black circles, left y axis) and on the final grafting efficiency (filled red squares, right y axis); bottom figure: effect of the reaction temperature on the final number average molecular weight of the free polymer (filled black circles, left y axis) and on the ratio of the final number average molecular weight of the grafted polymer over that of the free polymer (dashed red line, right y axis). (BPO/St 5 $\%wt$ for 50% GTR; reaction time = 120 min).

In Figure 10, the variation of the same quantities is plotted with respect to the reaction temperature, for constant GTR and BPO contents (i.e., BPO/St = 5 $\%wt$ and 50% GTR). In this case, a different behavior is observed as the final (i.e., after 120 min of reaction) monomer conversion and M_n initially remain relatively constant, for temperatures lower than 100-110 °C, and then display a rather rapid increase (for monomer conversion) and decrease (for M_n), respectively. At the same time, the ratio of the final M_n of the grafted

polymer over that of the free polymer displays a behavior similar to the one of monomer conversion, while the final grafting efficiency increases rapidly and reaches a value close to 100%, already at a temperature of about 120 °C. In fact, at lower temperatures, the mild increase of the rate of radical production with temperature seems to be counterbalanced by the parallel increase of the rates of radical termination and deactivation, thus limiting the monomer conversion and molecular weight at a constant level. However, as the temperature rises to values higher than 100-110 °C, the rate of creation of new radicals, both by the very rapid decomposition of the initiator and the thermal initiation mechanism, increases exponentially. Monomer propagation rates also increase. At the same time, the increase in the radical deactivation rate becomes limited by the saturation of the active sites of carbon black, thus allowing the system to reach high monomer conversion rates very rapidly, before complete consumption of the initiator. The increased number of radicals also contributes to the decrease of M_n. On the other hand, as the rate of propagation of the grafted radicals becomes significantly more important than the relative propagation rate of the free polymer (cf. Table 2), the respective average molecular weight constantly increases and so does the grafting efficiency as well. As a result, at very high temperatures and for the given GTR and BPO contents, the polymerization seems to take place principally on the grafted chains instead of the free radicals.

Figures 9 and 10 provide insights about the trends of the plotted magnitudes that are useful mainly within the perspective of a qualitative analysis. Note, however, that, as mentioned previously in section 4.5, the parametric estimation of the constants related to the grafting mechanisms, affecting the

values of molecular weights and grafting efficiency in a copolymerization system, has been carried out solely on the basis of monomer conversion data (i.e., the only available data). As such, the actual values predicted by the model for the molecular weights, in the presence of GTR, should be considered with caution. In fact, the experimental measurement of the molecular weight of the free polymer and of the grafting efficiency, requires an initial step of separation of the free polymer (and the remaining monomer) from the grafted polymer and the GTR particles. This step is typically carried out via solvent extraction. Then, the molecular weight can be determined by size exclusion chromatography while grafting efficiency can be calculated by gravimetric analysis [11, 26]. In this work, given that all copolymerization experiments were carried out at milligram scale during the DSC experiments, such analyses were not carried out. On the other hand, the molar mass of the grafted polymer cannot be experimentally measured by the above procedure, since the remaining mixture of GTR and grafted polymer is insoluble. In this respect, a kinetic model that can accurately predict the evolution of the polymerization under varying conditions, becomes of even greater importance in the analysis and understanding of such systems.

Finally, the predictions of the model have been tested against experimental DSC data for different reaction temperatures, as shown in Figure 11. More specifically, the evolution of monomer conversion under varying GTR and BPO contents is compared to the model predictions for two additional temperatures (i.e., besides the temperature considered in Figures 4-6, equal to 90°C), namely at 85°C and 120°C. The comparison further validates the capacity of the proposed model to capture the behavior of the system, in

the presence of GTR, under different conditions and up to relatively high temperatures.

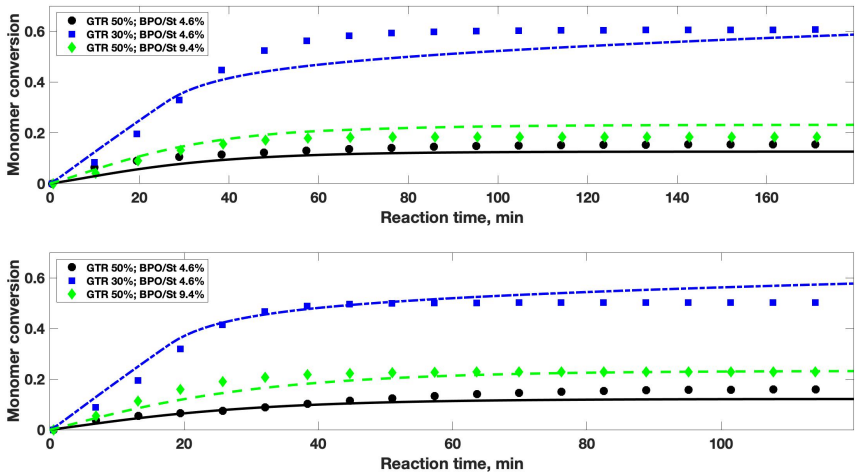

Figure 11: Evolution of monomer conversion, during the isothermal BPO-initiated polymerization of styrene in the presence of GTR particles, under different temperatures [23]. Upper figure: T = 85 °C; lower figure: T = 120 °C. (Filled circles and solid curves: BPO/St 4.6 %*wt* with 50% GTR; filled squares and dot/dashed curves: BPO/St 4.6 %*wt* with 30% GTR; filled diamonds and dashed curves: BPO/St 9.4 %*wt* with 50% GTR).

6. Conclusions

The radical polymerization of styrene in the presence of ground-tire rubber particles is a system that displays significant deviation from the respective pure styrene homopolymerization case, when a peroxide initiator is used. This deviation has been attributed to various factors, notably associated with the presence of highly-reacting additives in the formulation of GTR, such as carbon black, and with its three-dimensional network structure [23]. In this respect, a unified mathematical modeling framework, capable of predicting

the behavior of the system both in the absence and in the presence of GTR and under different conditions in terms of GTR content, initiator content and reaction temperature, would be extremely valuable to the relative research in this field.

The modeling framework proposed in this work attempted to respond to this exact need. In this sense, a general and comprehensive kinetic scheme was proposed to describe all the kinetic developments taking place in the system, on the basis of previously established models on styrene polymerization. A series of additional chemical reactions were included to account for the accelerated decomposition of peroxide radicals as well as for the grafting and the deactivation (partial and total) of the chain radicals. The diffusion-controlled phenomena were also incorporated in the model.

The proposed model was capable of describing the available polymerization data with high accuracy and of capturing the effects of the GTR and initiator content under different polymerization temperatures. Additional simulation runs were implemented to further illustrate the predicted effects of the different reaction conditions on the monomer conversion, molecular weight and grafting efficiency developments. Overall, the presence of GTR particles in the reacting system seems to affect mostly the reactions of initiation and termination via the acceleration of both decomposition of BPO and deactivation of the formed radicals, in parallel to the formation of grafted polymer chains. The generality of the kinetic scheme of the proposed framework allows further development and validation in the light of new data for the polymerization system under study, and makes it suitable for implementation in other similar systems employing different monomers and/or

initiators.

7. Acknowledgements

The authors acknowledge the valuable contribution of Dr. Alexandros Kiparissides, from the University College London (UCL), on the parametric estimation of the model.

Nomenclature

Greek Characters

α Reduced-mobility multiplicative coefficient

α_m Monomer thermal expansion coefficient (K^{-1})

α_p Polystyrene thermal expansion coefficient (K^{-1})

δ Average chain root mean square end-to-end distance (m)

δ_c Segmental diffusion parameter for styrene ($l.g^{-1}$)

λ_k Moment of the number-chain-length distribution of the free radicals, of order k ($mol.l^{-1}$)

μ_k Moment of the number-chain-length distribution of the free polymers, of order k ($mol.l^{-1}$)

ν_k Moment of the number-chain-length distribution of the grafted radicals, of order k ($mol.l^{-1}$)

ω_k Moment of the number-chain-length distribution of the reduced-activity grafted radicals, of order k ($mol.l^{-1}$)

σ Lennard Jones diameter (m)

θ_k Moment of the number-chain-length distribution of the reduced-activity free radicals, of order k ($mol.l^{-1}$)

ξ_k Moment of the number-chain-length distribution of the grafted polymers, of order k ($mol.l^{-1}$)

Symbols

A Adjustable parameter for the onset of the 2^{nd} stage of gel-effect

AH Diels-Alder adduct

AR 1-Phenyltetraryl radical

B Adjustable parameter for the onset of the 3^{rd} stage of gel-effect

C Adjustable parameter for the onset of the 4^{th} stage of gel-effect

CB Carbon black

D_n Polymer of chain length 'n'

DPR Deactivated primary-radical

f_1 Efficiency factor of chemical initiation

f_2 Efficiency factor of CB-induced initiation

f_{GTR} Efficiency factor of the GTR double bonds

GD_n Grafted polymer of chain length 'n'

GP_n Reduced-activity grafted radical of chain length 'n'

GPR Grafted primary-radical

GR_n Grafted radical of chain length 'n'

$GRat_c$ Critical value of mass fraction of GTR in the reacting mixture

I Initiator agent

j_c Average number of monomer units between chain entaglements (m

k kinetic rate constant (units: mol; l; min)

M Monomer, styrene

M_0 Molecular mass of styrene ($g.mol^{-1}$)

M_{DB} Initial molar concentration of double bonds of GTR ($mol.l^{-1}$)

MR Styryl radical

n_S Molar quantity of species S (mol)

P_n Reduced-activity free radical of chain length 'n'

PR Free primary radical

PRl Reduced-activity primary-radical

R_n Free radical of chain length 'n'

r_X Net formation rate of species X ($mol.min^{-1}.l^{-1}$)

V Volume of the reacting mixture (l)

GRat Mass fraction of GTR in the reacting mixture

Subscripts of the kinetic constants

-1 Diels-Alder dimerization inverse reaction

1 Diels-Alder dimerization forward reaction

2 Thermal initiation reaction from AH

A	Thermal initiation reaction from AR
B	Thermal initiation reaction from MR
C	Trimerization reaction
d	Initiator decomposition reaction
dCB	CB-induced decomposition reaction
dea	Radical deactivation reaction
fx	Transfer reaction to species 'x'
I	Initiation reaction
p	Propagation reaction
S	Scission reaction
tc	Termination by combination reaction
td	Termination by dispropportionation reaction
tPR	Transfer reaction to primary-radicals
xG	Grafting reaction analogous to the respective free radical mechanism 'x'

References

[1] S. Ramarad, M. Khalid, C. T. Ratnam, A. L. Chuah, W. Rashmi, Waste tire rubber in polymer blends: A review on the evolution, properties and future, Progress in Materials Science 72 (2015) 100–140. doi:10.1016/j.pmatsci.2015.02.004.

[2] D. Dobrotă, G. Dobrotă, An innovative method in the regeneration of waste rubber and the sustainable development, Journal of Cleaner Production 172 (2018) 3591–3599. doi:10.1016/j.jclepro.2017.03.022.

[3] H. L. Liu, X. P. Wang, D. M. Jia, Recycling of waste rubber powder by mechano-chemical modification, Journal of Cleaner Production 245 (2020). doi:10.1016/j.jclepro.2019.118716.

[4] J. E. Mark, B. Erman, M. C. Roland, The Science and Technology of Rubber, volume 1, 4th ed., Elsevier, Oxford, 2013. doi:10.1017/CBO9781107415324.004.

[5] D. Priddy, Styrene Polymers, volume 4, 2001. doi:10.1002/0471440264.pst354.

[6] D. Tuchman, S. L. Rosen, the Mechanical Properties of Plastics Containing Cryogenically Ground Tire, Journal of Elastomers and Plastics 10 (1978) 115–128.

[7] J. Karger-Kocsis, L. Mészáros, T. Bárány, Ground tyre rubber (GTR) in thermoplastics, thermosets, and rubbers, volume 48, 2013. doi:10.1007/s10853-012-6564-2.

[8] G. R. Meira, C. V. Luciani, D. A. Estenoz, Continuous Bulk Process for the Production of High-Impact Polystyrene: Recent Developments in Modeling and Control, Macromolecular Reaction Engineering 1 (2007) 25–39. doi:10.1002/mren.200600010.

[9] R. P. Burford, M. Pittolo, Rubber-crumb modified polystyrene. Part 2: Fracture toughness, Journal of Materials Science 21 (1986) 2308–2314.

[10] M. Pittolo, R. P. Burford, Rubber-crumb modified polystyrene. Part 1: Tensile properties, Journal of Materials Science 21 (1986) 1769–1774. doi:10.1007/bf01114738.

[11] S. Coiai, E. Passaglia, F. Ciardelli, D. Tirelli, F. Peruzzotti, E. Resmini, Modification of cross-linked rubber particles by free radical polymerization, Macromolecular Symposia 234 (2006) 193–202. doi:10.1002/masy.200650225.

[12] A. Brydon, G. M. Burnett, G. G. Cameron, Free-Radical Grafting of Monomers To Polydienes - I. Effect of Reaction Conditions on Grafting of Styrene To Polybutadiene., J Polym Sci Part A-1 Polym Chem 11 (1973) 3255–3269.

[13] R. Xiong, Studies in polymer composites based on carbon containing pulverized rubber materials, Doctor of philosophy in chemical engineering, Illinois Institute of Technology, 2010.

[14] E. L. Rodriguez, The effect of free radical initiators and fillers on the cure of unsaturated polyester resins, Polymer Engineering & Science 31 (1991) 1022–1028. doi:10.1002/pen.760311405.

[15] K. Fujiki, N. Tsubokawa, Y. Sone, Radical Grafting from Carbon Black. Graft Polymerization of Vinyl Monomers Initiated by Azo Groups Introduced onto Carbon Black Surface, Polymer Journal 22 (1990) 661–670.

[16] G. Kraus, T. Gruver, J., K. W. Rollmann, Polymerization by Carbon Blacks, Journal of Polymer Science XXXVI (1959) 564–565.

[17] K. Ohkita, N. Tsubokawa, E. Saitoh, M. Noda, N. Takashina, The free radical polymerization of vinyl monomers in the presence of carbon black, Carbon 13 (1975) 443–448. doi:10.1016/0008-6223(75)90017-2.

[18] K. Ohkita, N. Tsubokawa, E. Saitoh, The competitive reactions of initiator fragments and growing polymer chains against the surface of carbon black, Carbon 16 (1978) 41–45. doi:10.1016/0008-6223(78)90114-8.

[19] J. Yan, X. Miao, Q. Zhang, X. Cui, J. Li, H. Wang, One-Step Preparation of Black Polystyrene Particles via In Situ Suspension Polymerization, Polymer Engineering and Science (2011) 294–301. doi:10.1002/pen.

[20] J. Yan, W. Chunlei, Y. Gao, Z. Zheng, Z. Cheng, X. Cui, H. Wang, Experimental Investigation on the Role of PVA in Eliminating Inhibition Phenomenon of Carbon Black During the Synthesis of Polystyrene/Carbon Black Composite Particles, Polymer Engineering and Science (2012). doi:10.1002/pen.

[21] N. Tsubokawa, K. Fujiki, Y. Sone, Radical Grafting from Carbon Black. Graft Polymerization of Vinyl Monomers Initiated by Peroxyester Groups Introduced, Polymer Journal 20 (1988) 213–220.

[22] J. Ueda, H. Yamaguchi, K. Shirai, T. Yamauchi, N. Tsubokawa, Radical Polymerization of Vinyl Monomers in the Presence of Carbon Black Initiated by 2,2'-Azobisisobutyronitrile and Benzoyl Peroxide in Ionic Liquid, Journal of Applied Polymer Science 107 (2008) 3300–3305. doi:10.1002/app.27448.

[23] D. Florez, S. Hoppe, G. H. Hu, D. Meimaroglou, Radical bulk polymerization of styrene in the presence of rubber particles from recycled tires: a kinetic study using DSC, Journal of Thermal Analysis and Calorimetry (2020). doi:10.1007/s10973-020-09701-z.

[24] T. Alfrey, C. C. Price, Relative reactivities in vinyl copolymerization, Journal of Polymer Science 2 (1947) 101–106. doi:10.1002/pol.1947.120020112.

[25] M.-J. Wang, C. A. Gray, S. R. Reznek, K. Mahmud, Y. Kutsovsky, Vol. 9 Carbon Black, 2005.

[26] D. C. Florez Parra, Effects of the presence of recycled tire powders on the kinetics of the radical polymerization of styrene and the properties of the resulting materials, Ph.D. thesis, University of Lorraine, 2019.

[27] A. E. Hamielec, J. W. Hodgins, K. Tebbens, Polymer Reactors and Molecular Weight Distribution: Part II. Free Radical Polymerization in a Batch Reactor, AIChE Journal 13 (1967) 1087–1091. doi:10.1002/app.1969.070130705.

[28] J. H. Duerksen, A. E. Hamielec, J. W. Hodgins, Polymer reactors and molecular weight distribution: Part I. Free radical polymerization in a

continuous stirred-tank reactor, AIChE Journal 13 (1967) 1081–1086. doi:10.1002/aic.690130609.

[29] A. W. Hui, A. E. Hamielec, Thermal polymerization of styrene at high conversions and temperatures. An experimental study, Journal of Applied Polymer Science 16 (1972) 749–769. doi:10.1002/app.1972.070160319.

[30] A. Husain, A. E. Hamielec, Thermal polymerization of styrene, Journal of Applied Polymer Science 22 (1978) 1207–1223. doi:10.1002/app.1978.070220505.

[31] F. R. Mayo, The dimerization of styrene, Journal of the American Chemical Society 90 (1968) 1289–1295.

[32] F. L. Marten, A. E. Hamielec, High-Conversion Diffusion-Controlled Polymerization of Styrene. I, Journal of Applied Polymer Science 27 (1982) 489–505.

[33] D. S. Achillas, C. Kiparissides, Development of a General Mathematical Framework for Modeling Diffusion-Controlled Free-Radical Polymerization Reactions, Macromolecules 25 (1992) 3739–3750. doi:10.1021/ma00040a021.

[34] N. Tefera, G. Weickert, K. R. Westerterp, Modeling of free radical polymerization up to high conversion. II. Development of a mathematical model, Journal of Applied Polymer Science 63 (1997) 1663–1680.

[35] J. Gao, K. D. Hungenberg, A. Penlidis, Process modelling and optimization of styrene polymerization, Macromolecular Symposia 206 (2004) 509–522. doi:10.1002/masy.200450239.

[36] M. J. Scorah, R. Dhib, A. Penlidis, Modelling of free radical polymerization of styrene and methyl methacrylate by a tetrafunctional initiator, Chemical Engineering Science 61 (2006) 4827–4859. doi:10.1016/j.ces.2006.03.018.

[37] C. Kotoulas, A. Krallis, P. Pladis, C. Kiparissides, A comprehensive kinetic model for the combined chemical and thermal polymerization of styrene up to high conversions, Macromolecular Chemistry and Physics 204 (2003) 1305–1314. doi:10.1002/macp.200390104.

[38] J. D. Woloszyn, K. B. Mcauley, Application of Parameter Selection and Estimation Techniques in a Thermal Styrene Polymerization Model, Macromolecular Reaction Engineering 5 (2011) 453–466. doi:10.1002/mren.201100021.

[39] J. D. Woloszyn, P. Hesse, K. D. Hungenberg, K. B. Mcauley, Parameter selection and estimation techniques in a styrene polymerization model, Macromolecular Reaction Engineering 7 (2013) 293–310. doi:10.1002/mren.201200074.

[40] P. Manaresi, V. Passalacqua, F. Pilati, Kinetics of graft polymerization of styrene on cis-1,4-polybutadiene, Polymer 16 (1975) 520–526. doi:10.1016/0032-3861(75)90011-7.

[41] A. Brydon, G. M. Burnett, G. G. Cameron, Free-Radical Grafting of Monomers To Polydienes - 2. Kinetics and Mechanism of Styrene Grafting To Polybutadiene., J Polym Sci Part A-1 Polym Chem 12 (1974) 1011–1021.

[42] G. G. Cameron, M. Y. Qureshi, Free Radical Grafting of Monomers To Polydienes - 3. Kinetics and Mechanism of Styrene Grafting To Polyisoprene., Journal of polymer science. Part A-1, Polymer chemistry 18 (1980) 2143–2153. doi:10.1002/pol.1980.170181102.

[43] N. J. Huang, D. C. Sundberg, Fundamental studies of grafting reactions in free radical copolymerization. I. A detailed kinetic model for solution polymerization, Journal of Polymer Science Part A: Polymer Chemistry 33 (1995) 2533–2549. doi:10.1002/pola.1995.080331502.

[44] N. J. Huang, D. C. Sundberg, Fundamental studies of grafting reactions in free radical copolymerization. IV. Grafting of styrene, acrylate, and methacrylate monomers onto vinyl-polybutadiene using benzoyl peroxide and AIBN initiators in solution polymerization., Journal of Polymer Science Part A: Polymer Chemistry 33 (1995) 2587–2603. doi:10.1002/pola.1995.080331505.

[45] N. J. Huang, D. C. Sundberg, Fundamental studies of grafting reactions in free radical copolymerization. II. Grafting of styrene, acrylate, and methacrylate monomers onto cis-polybutadiene using AIBN initiator in solution polymerization, Journal of Polymer Science Part A: Polymer Chemistry 33 (1995) 2551–2570. doi:10.1002/pola.1995.080331503.

[46] N. J. Huang, D. C. Sundberg, Fundamental studies of grafting reactions in free radical copolymerization. III. Grafting of styrene, acrylate, and methacrylate monomers onto cis-polybutadiene using benzoyl peroxide initiator in solution polymerization, Journal of Polymer Science Part A: Polymer Chemistry 33 (1995) 2571–2586. doi:10.1002/pola.1995.080331504.

[47] D. A. Estenoz, G. R. Meira, N. Gomez, , O. H. M., Mathematical model of a continuous industrial high-impact polystyrene process, AIChE Journal 44 (1998) 427–441. doi:10.1002/aic.690440219.

[48] F. L. Figueira, Y.-Y. Wu, Y.-N. Zhou, Z.-H. Luo, P. H. M. Van Steenberge, D. R. D'hooge, Coupled matrix kinetic Monte Carlo simulations applied for advanced understanding of polymer grafting kinetics, Reaction Chemistry & Engineering 6 (2021) 640–661. doi:10.1039/D0RE00407C.

[49] Y. Y. Wu, F. L. Figueira, P. H. Van Steenberge, D. R. D'hooge, Y. N. Zhou, Z. H. Luo, Bridging principal component analysis and method of moments based parameter estimation for grafting of polybutadiene with styrene, Chemical Engineering Journal 425 (2021) 130463. doi:10.1016/J.CEJ.2021.130463.

[50] J. L. White, A. Sasaki, Free radical graft polymerization, Polymer - Plastics Technology and Engineering 42 (2003) 711–735. doi:10.1081/PPT-120024992.

[51] D. Elizarrarás, G. Morales, R. Díaz De León, C. Luciani, D. Es-

tenoz, A mathematical model of the bulk copolymerization of styrene and acrylonitrile in the presence of polystyrene-block-polybutadiene, Macromolecular Theory and Simulations 17 (2008) 180–197. doi:10.1002/mats.200800004.

[52] C. Gutierrez, D. A. Estenoz, L. M. Gugliotta, J. R. Vega, G. R. Meira, Solution and Quasi-Bulk Copolymerizations of Styrene and Methyl Methacrylate in the Presence of Polybutadiene: Mathematical Model, Journal of Applied Polymer Science 117 (2010) 899–919. doi:10.1002/app.31403.

[53] G. Odian, Radical Chain Polymerization, in: Principles of Polymerization, 4 ed., John Wiley & Sons, Ltd, 2004, pp. 198–349. doi:10.1002/047147875X.CH3.

[54] K. Konstadinidis, D. S. Achilias, C. Kiparissides, Development of a unified mathematical framework for modelling molecular and structural changes in free-radical homopolymerization reactions, Polymer 33 (1992) 5019–5031. doi:10.1016/0032-3861(92)90053-Y.

[55] G. G. Cameron, M. Y. Qureshi, Free Radical Grafting of Monomers To Polydienes - 4. Kinetics and Mechanism of Methyl Methacrylate Grafting To Polybutadiene., Journal of polymer science. Part A-1, Polymer chemistry 18 (1980) 3149–3161. doi:10.1002/pol.1980.170181102.

[56] M. A. Villalobos, A. E. Hamielec, P. E. Wood, Bulk and suspension polymerization of styrene in the presence of n-pentane. An evaluation of

monofunctional and bifunctional initiation, Journal of Applied Polymer Science 50 (1993) 327–343. doi:10.1002/app.1993.070500214.

[57] J. C. Lagarias, J. A. Reeds, M. H. Wright, P. E. Wright, Convergence Properties of the Nelder-Mead Simplex Method in Low Dimensions, SIAM Journal of Optimization 9 (1998) 112–147.

[58] D. R. D'hooge, M. F. Reyniers, G. B. Marin, The crucial role of diffusional limitations in controlled radical polymerization, Macromolecular Reaction Engineering 7 (2013) 362–379. doi:10.1002/MREN.201300006.

[59] L. De Keer, P. H. M. Van Steenberge, M.-F. Reyniers, G. B. Marin, K.-D. Hungenberg, L. Seda, D. R. D'hooge, A complete understanding of the reaction kinetics for the industrial production process of expandable polystyrene, AIChE Journal 63 (2017) 2043–2059. doi:10.1002/AIC.15587.

[60] C. Barner-Kowollik, P. Vana, T. P. Davis, The Kinetics of Free-Radical Polymerization, in: Handbook of Radical Polymerization, John Wiley & Sons, Ltd, 2003, pp. 187–261. doi:10.1002/0471220450.CH4.

[61] L. De Keer, F. L. Figueira, Y. W. Marien, K. De Smit, M. Edeleva, P. H. Van Steenberge, D. R. D'hooge, Benchmarking Stochastic and Deterministic Kinetic Modeling of Bulk and Solution Radical Polymerization Processes by Including Six Types of Factors Two, Macromolecular Theory and Simulations 29 (2020) 2000065. doi:10.1002/MATS.202000065.

[62] R. C. Zabisky, W. M. Chan, P. E. Gloor, A. E. Hamielec, A kinetic model for olefin polymerization in high-pressure tubular reactors: a review and

update, Polymer 33 (1992) 2243–2262. doi:10.1016/0032-3861(92)90514-W.

Appendix A. Model Equations

Appendix A.1. Rate functions of the macromolecular species

The net formation rates of all the macromolecular species that participate in the different chemical reactions can be established, on the basis of the postulated general kinetic scheme (Eqs.(1)-(40)), as follows:

- Free polymer, D_n

$$
\begin{aligned}
r_{D_n} = {} & k_C \cdot [AH] \cdot [M] \cdot \delta(n-3) + (k_{fm} \cdot [M] + k_{fAH} \cdot [AH]) \cdot [R_n] \\
& + k_s \cdot [PR] \cdot \left(\sum_{k=n+1}^{\infty} [D_k] - (n-1) \cdot [D_n] \right) + k_{tPR} \cdot [PR] \cdot [R_n] \\
& + \frac{1}{2} k_{tc} \cdot \sum_{k=1}^{n-1} [R_k] \cdot [R_{n-k}] + k_{td} \cdot [R_n] \cdot \sum_{k=1}^{\infty} [R_k] + k_{fG} \cdot [G] \cdot [R_n] \\
& + k_{tdG} \cdot [R_n] \cdot \sum_{k=1}^{\infty} [GR_k] + k_{dea} \cdot [CB] \cdot ([R_n] + \alpha \cdot [P_n]) \\
& + \alpha \cdot \left(\frac{1}{2} k_{tc} \cdot \left(\alpha \cdot \sum_{k=1}^{n-1} [P_k] \cdot [P_{n-k}] + 2 \cdot \sum_{k=1}^{n-1} [R_k] \cdot [P_{n-k}] \right) \right) \\
& + \alpha \cdot k_{td} \cdot \left(\alpha \cdot [P_n] \cdot \sum_{k=1}^{\infty} [P_k] + [R_n] \cdot \sum_{k=1}^{\infty} [P_k] + [P_n] \cdot \sum_{k=1}^{\infty} [R_k] \right) \\
& + \alpha \cdot k_{tdG} \cdot \left(([R_n] + \alpha \cdot [P_n]) \cdot \sum_{k=1}^{\infty} [GP_k] + [P_n] \cdot \sum_{k=1}^{\infty} [GR_k] \right) \\
& + k_{dea} \cdot [CB] \cdot ([MR] \cdot \delta(n-1) + [AR] \cdot \delta(n-2))
\end{aligned}
\tag{A.1}
$$

- Grafted radicals, GR_n

$$\begin{aligned} r_{GR_n} = & (k_pG \cdot [GPR] \cdot [M]) \cdot \delta(n-1) + k_pG \cdot [M] \cdot ([GR_{n-1}] - [GR_n]) \\ & - (k_{fmG} \cdot [M] + k_{fAHG} \cdot [AH]) \cdot [GR_n] \\ & - (k_{tcG} + k_{tdG}) \cdot [GR_n] \cdot \left(\sum_{k=1}^{\infty} [R_k] + \alpha \cdot \sum_{k=1}^{\infty} [P_k] \right) \\ & - k_{tPRG} \cdot [PR] \cdot [GR_n] - k_{deaG} \cdot [CB] \cdot [GR_n] \end{aligned} \tag{A.2}$$

- Grafted polymer, GD_n

$$\begin{aligned} r_{GD_n} = & (k_{fmG} \cdot [M] + k_{fAHG} \cdot [AH]) \cdot [GR_n] \\ & + k_{tcG} \cdot \sum_{k=1}^{n-1} [R_k] \cdot [GR_{n-k}] + k_{tdG} \cdot [GR_n] \cdot \sum_{k=1}^{\infty} [R_k] \\ & + k_{tPRG} \cdot [PR] \cdot [GR_n] + k_{deaG} \cdot [CB] \cdot ([GR_n] + \alpha \cdot [GP_n]) \\ & + \alpha \cdot k_{tcG} \cdot \left(\sum_{k=1}^{n-1} [GR_k] \cdot [P_{n-k}] + \sum_{k=1}^{n-1} [R_k] \cdot [GP_{n-k}] + \alpha \cdot \sum_{k=1}^{n-1} [P_k] \cdot [GP_{n-k}] \right) \\ & + \alpha \cdot k_{tdG} \cdot \left(\alpha \cdot [GP_n] \cdot \sum_{k=1}^{\infty} [P_k] + [GP_n] \cdot \sum_{k=1}^{\infty} [R_k] + [GR_n] \cdot \sum_{k=1}^{\infty} [P_k] \right) \end{aligned} \tag{A.3}$$

- Reduced-activity free radicals, P_n

$$\begin{aligned} r_{P_n} = & (\alpha \cdot k_I \cdot [M] \cdot [PRl]) \cdot \delta(n-1) \\ & + \alpha \cdot k_p \cdot [M] \cdot ([P_{n-1}] - [P_n]) - \alpha^2 \cdot (k_{tc} + k_{td}) \cdot [P_n] \cdot \sum_{k=1}^{\infty} [P_k] \\ & - \alpha \cdot \left((k_{tc} + k_{td}) \cdot \sum_{k=1}^{\infty} [R_k] + (k_{tcG} + k_{tdG}) \cdot \left(\sum_{k=1}^{\infty} [GR_k] + \alpha \cdot \sum_{k=1}^{\infty} [GP_k] \right) \right) \cdot [P_n] \\ & - \alpha \cdot \ k_{dea} \cdot [P_n] \cdot [CB] \end{aligned} \tag{A.4}$$

- Reduced-activity grafted radicals, GP_n

$$r_{GP_n} = (\alpha \cdot k_{IG} \cdot [G] \cdot [PRl]) \cdot \delta(n-1) + \alpha \cdot k_{pG} \cdot [M] \cdot ([GP_{n-1}] - [GP_n]) - \alpha \cdot \left((k_{tcG} + k_{tdG}) \cdot \left(\sum_{k=1}^{\infty} [R_k] + \alpha \cdot \sum_{k=1}^{\infty} [P_k] \right) \right) \cdot [GP_n] - \alpha \cdot \ k_{deaG} \cdot [GP_n] \cdot [CB] \tag{A.5}$$

Note that the rate function for the free radicals has already been presented in section 4 (Eq.(41)). Note also that the derivation of these rate functions, on the basis of the postulated kinetic scheme, is subject to different interpretations, mostly with respect to the factors accompanying the terms corresponding to bimolecular reactions involving identical species (e.g., termination reactions). This is a phenomenon that is well established in the literature [53, 60, 61]. Accordingly, extreme care should be taken when adopting parts of reported mathematical models or their respective kinetic rate values.

Appendix A.2. Moment rate functions

In accordance to the definition given in Eq.(43), the moments μ_k, ν_k, ξ_k, θ_k and ω_k have been defined for the macromolecular species D_n, GR_n, GD_n, P_n and GP_n, respectively. Next, on the basis of the previously defined rate functions (Eqs.(A.1)-(A.5)) and according to the procedure followed previously for R_n (Eq.(44)), the following rate functions can be established for the leading moments of the number-chain-length distributions of the above macromolecular species:

- Moments of the free polymer, μ_k

$$
\begin{aligned}
r_{\mu_k} &= 3^k \cdot k_C \cdot [AH] \cdot [M] + (k_{fm} \cdot [M] + k_{fAH} \cdot [AH]) \cdot \lambda_k \\
&+ k_s \cdot [PR] \cdot (T_1 - (\mu_{k+1} - \mu_k)) + k_{tPR} \cdot [PR] \cdot \lambda_k \\
&+ \frac{1}{2} k_{tc} \cdot \sum_{r=0}^{k} \binom{k}{r} \lambda_r \cdot \lambda_{k-r} + k_{td} \cdot \lambda_k \cdot \lambda_0 \\
&+ k_{fG} \cdot [G] \cdot \lambda_k + k_{tdG} \cdot \lambda_k \cdot \nu_0 + k_{dea} \cdot [CB] \cdot (\lambda_k + \alpha \cdot \theta_k) \\
&+ \alpha \cdot \left(\frac{1}{2} k_{tc} \cdot \left(\alpha \cdot \sum_{r=0}^{k} \binom{k}{r} \theta_r \cdot \theta_{k-r} + 2 \cdot \sum_{r=0}^{k} \binom{k}{r} \lambda_r \cdot \theta_{k-r} \right) \right) \\
&+ \alpha \cdot k_{td} \cdot (\alpha \cdot \theta_k \cdot \theta_0 + \lambda_k \cdot \theta_0 + \theta_k \cdot \lambda_0) + \alpha \cdot k_{tdG} \cdot ((\lambda_k + \alpha \cdot \theta_k) \cdot \omega_0 + \theta_k \cdot \nu_0) \\
&+ k_{dea} \cdot [CB] \cdot ([MR] + 2 \cdot [AR])
\end{aligned}
\tag{A.6}
$$

- Moments of the grafted radicals, ν_k

$$
\begin{aligned}
r_{\nu_k} &= k_p G \cdot [GPR] \cdot [M] + k_p G \cdot [M] \cdot \left(\sum_{r=0}^{k} \binom{k}{r} \nu_r - \nu_k \right) - k_{tPRG} \cdot [PR] \cdot \nu_k \\
&- (k_{fmG} \cdot [M] + k_{fAHG} \cdot [AH]) \cdot \nu_k - (k_{tcG} + k_{tdG}) \cdot \nu_k \cdot (\lambda_0 + \alpha \cdot \theta_0) \\
&- k_{deaG} \cdot [CB] \cdot \nu_k
\end{aligned}
\tag{A.7}
$$

- Moments of the grafted polymer, ξ_k

$$
\begin{aligned}
r_{\xi_k} = {} & (k_{fmG} \cdot [M] + k_{fAHG} \cdot [AH]) \cdot \nu_k + k_{tdG} \cdot \nu_k \cdot \lambda_0 \\
& + k_{tcG} \cdot \sum_{r=0}^{k} \binom{k}{r} \lambda_r \cdot \nu_{k-r} + k_{tPRG} \cdot [PR] \cdot \nu_k \\
& + k_{deaG} \cdot [CB] \cdot (\nu_k + \alpha \cdot \omega_k) + \alpha \cdot k_{tdG} \cdot (\alpha\omega_k \cdot \theta_0 + \omega_k \cdot \lambda_0 + \nu_k \cdot \theta_0) \\
& + \alpha \cdot k_{tcG} \cdot \left(\sum_{r=0}^{k} \binom{k}{r} \nu_r \cdot \theta_{k-r} + \sum_{r=0}^{k} \binom{k}{r} \lambda_r \cdot \omega_{k-r} + \alpha \cdot \sum_{r=0}^{k} \binom{k}{r} \theta_r \cdot \omega_{k-r} \right)
\end{aligned}
\tag{A.8}
$$

- Moments of the reduced-activity free radicals, θ_k

$$
\begin{aligned}
r_{\theta_k} = {} & \alpha \cdot [M] \cdot \left(k_I \cdot [PRl] + k_p \cdot \left(\sum_{r=0}^{k} \binom{k}{r} \theta_r - \theta_k \right) \right) \\
& - \alpha \cdot ((k_{tc} + k_{td}) \cdot (\alpha \cdot \theta_0 + \lambda_0) + (k_{tcG} + k_{tdG}) \cdot (\nu_0 + \alpha \cdot \omega_0)) \cdot \theta_k \\
& - \alpha \cdot \ k_{dea} \cdot \theta_k \cdot [CB]
\end{aligned}
\tag{A.9}
$$

- Moments of the reduced-activity grafted radicals, ω_k

$$
\begin{aligned}
r_{\omega_k} = {} & \alpha \cdot \left(k_{IG} \cdot [G] \cdot [PRl] + k_{pG} \cdot [M] \cdot \left(\sum_{r=0}^{k} \binom{k}{r} \omega_r - \omega_k \right) \right) \\
& - \alpha \cdot \omega_k \cdot ((k_{tcG} + k_{tdG}) \cdot (\lambda_0 + \alpha \cdot \theta_0)) - \alpha \cdot \ k_{deaG} \cdot \omega_k \cdot [CB]
\end{aligned}
\tag{A.10}
$$

The definitions of the terms T_1 and T_{1G} are given in Eq.(45). Note that, some terms of the above rate functions create a dependency of a moment of order k on a moment of order k+1 (i.e., the so-called moment-closure problem). To overcome this problem and *close* the mass balances of the

system, the following closure technique has been adopted in this study, on the basis of an assumed log-normal distribution [62]:

$$\Phi_3 = \Phi_0 \cdot \left(\frac{\Phi_2}{\Phi_1}\right)^3 \tag{A.11}$$

where Φ_k denotes the moment of order k of any of the macromolecular species of the system. The above expression provided satisfactory mass balance closure (i.e., $\geq 99.9\%$) for all the tested systems and conditions.

Appendix A.3. Calculation of properties

The implementation of the method of moments provides a straightforward calculation of many average properties of interest of the various macromolecular species of the system. In this respect, the number- and weight-average molecular weights of the free polymer, D_n, will be directly calculated by:

$$M_n = \frac{\mu_1}{\mu_0} \cdot M_0 \quad ; \quad M_w = \frac{\mu_2}{\mu_1} \cdot M_0 \tag{A.12}$$

Accordingly, the respective properties of any of the macromolecular species, that are present in the reacting mixture, can be calculated at any instant of the polymerization.

Appendix B. Reduced Kinetic Scheme

All the model equations presented in the rest of this work correspond to the complete general kinetic scheme, as presented in Eqs.(1)-(40). In this section, a reduced kinetic scheme is presented, as established following the parametric estimation process (see Section 4).

In fact, as explained in Section 4.5, given the available experimental data, it would be meaningless to estimate the values of all the parameters corresponding to all the reactions of the postulated kinetic scheme. In addition, some of these reactions have been considered negligible in the tested conditions (e.g., termination by disproportionation, termination by primary radicals, scission reactions, see Section 4.5). Accordingly, the general kinetic scheme, under the conditions and data considered in this work, can be reduced to the following kinetic scheme:

- Chemical initiation

$$I \xrightarrow{k_d, f_1} 2PR \tag{B.1}$$

$$I + CB \xrightarrow{k_{dCB}, f_2} PRl \tag{B.2}$$

$$M/G + PR \xrightarrow{k_I/k_{IG}} R_1/GPR \tag{B.3}$$

$$M + GPR \xrightarrow{k_{pG}} GR_1 \tag{B.4}$$

$$M/G + PRl \xrightarrow{\alpha \cdot k_I/k_{IG}} P_1/GP_1 \tag{B.5}$$

- Thermal initiation

$$2M \underset{k_{-1}}{\overset{k_1}{\longleftrightarrow}} AH \tag{B.6}$$

$$AH + M \xrightarrow{k_2} AR + MR \tag{B.7}$$

$$AR/MR + M \xrightarrow{k_A/K_B} R_3/R_2 \tag{B.8}$$

$$AH + M \xrightarrow{k_C} D_3 \tag{B.9}$$

- Propagation:

$$M + R_n(GR_n) \xrightarrow{k_p/k_{pG}} R_{n+1}/GR_{n+1} \tag{B.10}$$

$$M + P_n/GP_n \xrightarrow{\alpha \cdot k_p/k_{pG}} P_{n+1}/GP_{n+1} \tag{B.11}$$

- Transfer:

$$M + R_n \xrightarrow{k_{fm}} D_n + R_1 \tag{B.12}$$

$$AH + R_n \xrightarrow{k_{fAH}} D_n + AR \tag{B.13}$$

- Termination:

$$R_n + R_m/GR_m \xrightarrow{k_{tc}/k_{tcG}} D_{n+m}/GD_{n+m} \tag{B.14}$$

$$R_n/GR_n + P_m \xrightarrow{\alpha \cdot k_{tc}/\alpha \cdot k_{tcG}} D_{n+m}/GD_{n+m} \tag{B.15}$$

$$R_n + GP_m \xrightarrow{\alpha \cdot k_{tcG}} GD_{n+m} \tag{B.16}$$

$$P_n + P_m \xrightarrow{\alpha^2 \cdot k_{tc}} D_{n+m} \tag{B.17}$$

- Radical deactivation by carbon black:

$$PR/GPR + CB \xrightarrow{k_{dea}} DPR \tag{B.18}$$

$$MR/AR + CB \xrightarrow{k_{dea}} D_1/D_2 \tag{B.19}$$

$$CB + R_n/P_n \xrightarrow{k_{dea}/\alpha \cdot k_{dea}} D_n \tag{B.20}$$

$$CB + GR_n/GP_n \xrightarrow{k_{deaG}/\alpha \cdot k_{deaG}} GD_n \tag{B.21}$$